Doctoral Dissertation

Kinetic model expressing the anomalous phenomenon in human induced pluripotent stem cell (hiPSC) culture

Nguyen Thi Nhu Trang

January 2021

Graduate School of Engineering

Osaka University

Contents

Chapter 1 General Introduction

1.1 Kinetic modelling of biological systems

In physics and chemistry, kinetic models have been used to study system dynamics since the 18th century (Wisniak 2005, Oliveira et al. 2016), but have only begun receiving attention from biologists since the 20th century (Bailey and Ollis 1986, Grima and Schnell 2008). Thus, many methodologies, algorithms, and theoretical models used in physics and chemistry have been applied for establishing kinetic models in biological field (Gruebele and Thirumalai 2013). The most well-known models in early stage of biological modelling are Michaelis-Menten model which describes the enzyme-catalyzed reactions (Michaelis and Menten 1913) and Monod model for the growth of microorganisms (Monod 1949). Modelling biological systems is more difficult than modelling physical or chemical systems due to the stochastic nature of, intrinsic multi-scale, and fluctuations within biological processes (Resat et al. 2009). In 1999, McAdams et al. showed the importance of stochastic biochemical reactions in guarantee of biological systems' functions. The multiscale of biological system comes from the interactions of many elements at different levels from molecular, cellular, tissue, body, to society. The low copy numbers of biological objects lead to high fluctuations in biological systems. Despite those difficulties, once a biological system is described by an adequate model, researchers can have new insights into a particular problem, generate hypotheses, and design new experiments (Koide et al. 2009, Motta and Pappalardo 2012, Torres and Santos 2015). Simulating kinetic models on computer (*in silico* study) are speedy, economical, and able to easily satisfy many conditions that are impossible to be realized in reality (*e.g., in vitro* study) (**Fig. 1.1**).

Kinetic models have been applied to biological systems from subcellular scale, cellular scale, to tissue or whole organism scale (Martins et al. 2010, Castiglione et al. 2014). On the subcellular scale, modelers usually model gene regulatory networks or cell signaling pathways, and ordinary and partial differential equations are commonly selected to describe molecular

dynamics (Rangamani et al. 2013, Selekman et al. 2013, Deshpande and Spector 2017, Heydari et al. 2017, Yachie-Kinoshita et al. 2018). On the cellular scale, a single cell is usually considered as a unit black box, and interactions between cells rather than events occurring inside a cell are focused. In this situation, it is more effective to use discrete stochastic approaches such as agent-based models since they can describe the heterogeneity and fluctuations within a cell population (Schluter et al. 2014, Aland et al. 2015, Libby et al. 2019). Lastly, targets of multicellular scales are usually particular functional changes in an organ, organ system, or organism. In most cases, full description of system components is almost impossible, and differential equations are normally sufficient to model functions using physical or chemical laws (Taya et al. 1989, Hoehme et al. 2010, Jalali et al. 2015).

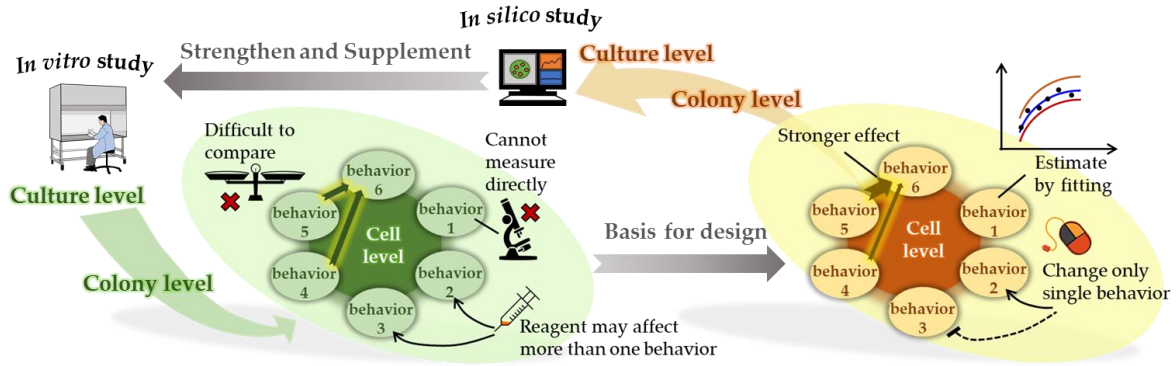

Figure 1.1 The relationship between *in vitro* study and *in silico* study in biological field. *In vitro* study focuses on new finding, while *in silico* study explores space not reachable by *in vitro* study.

1.2 Modelling approach

In general, models can be categorized into two groups: continuum models and agent-based models (Byrne and Drasdo 2008). Normally, continuum models are developed from ordinary or partial differential equations that describe the average of the whole cell population rather than individual cells. This kind of model is suitable for understanding the stability and general qualitative features of the cell population. Specially, conventional kinetic models in this group

for modelling cellular growth are classified as non-structured non-segregated model (e.g. Monod equation for growth of microorganisms), structured non-segregated model, and non-structured segregated model (**Fig. 1.2**). It is referred to as structured model when cell population is considered as multicomponent system instead of one component system (Bapat et al. 2006, Steuer et al. 2006). If the model describes cell to cell heterogeneity, it is considered as segregated model (Taya et al. 1989, Fordyce and Rawlings 1996). In real cell population, the situation is structured and segregated. When it comes to modelling, in most cases non-structured non-segregated models are used due to its simplicity (Bailley and Ollis, 1986).

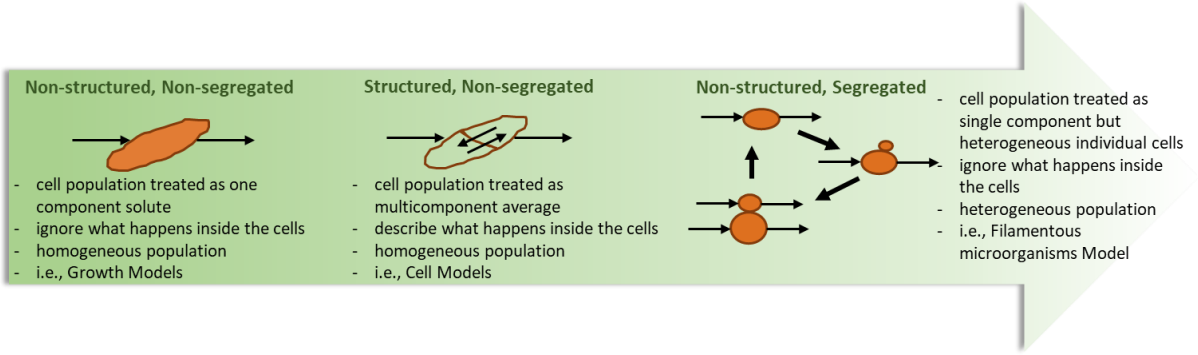

Figure 1.2 Different conventional modeling approaches for cell population kinetics (Bailey and Ollis,1986).

In contrast, agent-based models, including on-lattice models and off-lattice models, simulate the multicellular system at the single-cell level, and therefore, are more appropriate for quantitative analysis and describing the heterogeneity of a cell population (Metzcar et al. 2019, Nava-Sedeno et al. 2020). On-lattice models can be further categorized as lattice-gas cellular automata, cellular automata (CA), and cellular Potts model when one lattice element is occupied by more than one cell, exactly one cell, and less than one cell, respectively (Metzcar et al. 2019) (**Fig. 1.3**). In off-lattice models, cells can be at any location in the continuous space instead of being restricted by lattice (Hwang et al. 2009). In CA model, each lattice element takes one of a finite number of states (Moreira and Deutsch 2002). State of each lattice element is affected by its neighbors via the transition rules which can be deterministic or probabilistic.

Every lattice element updates its state simultaneously at each time step according to the transition rules. CA models are usually used in tissue engineering, tumor growth, and wound healing (Hwang et al. 2009). In these biological areas, some cell behaviors such as division, migration, and differentiation are commonly modeled. To model cell division, two important transitions rules relates to division probability (cell cycle time) and position to place daughter cell (Kino-oka et al. 2000, Yashiki et al. 2001, Cheng et al. 2006, Piotrowska and Angus 2009, Kagawa and Kino-oka 2016). For cell migration modelling, modelers need to decide the direction, rate, and probability of migration. Previously, transition rules for migration have been set by considering mechanical confinements, nutrients supply, and inhibitory ‘‘toxic’’ metabolites (Mansury and Deisboeck 2003), or concentrations of fibronectin, integrin, and cadherin (Robertson et al. 2007). In case of differentiation modelling, Checa and Prendergast (2009) determined whether mesenchymal stem cells would make a transition to fibroblasts, chondrocytes, or osteoblasts based on the level of mechanical stimulus.

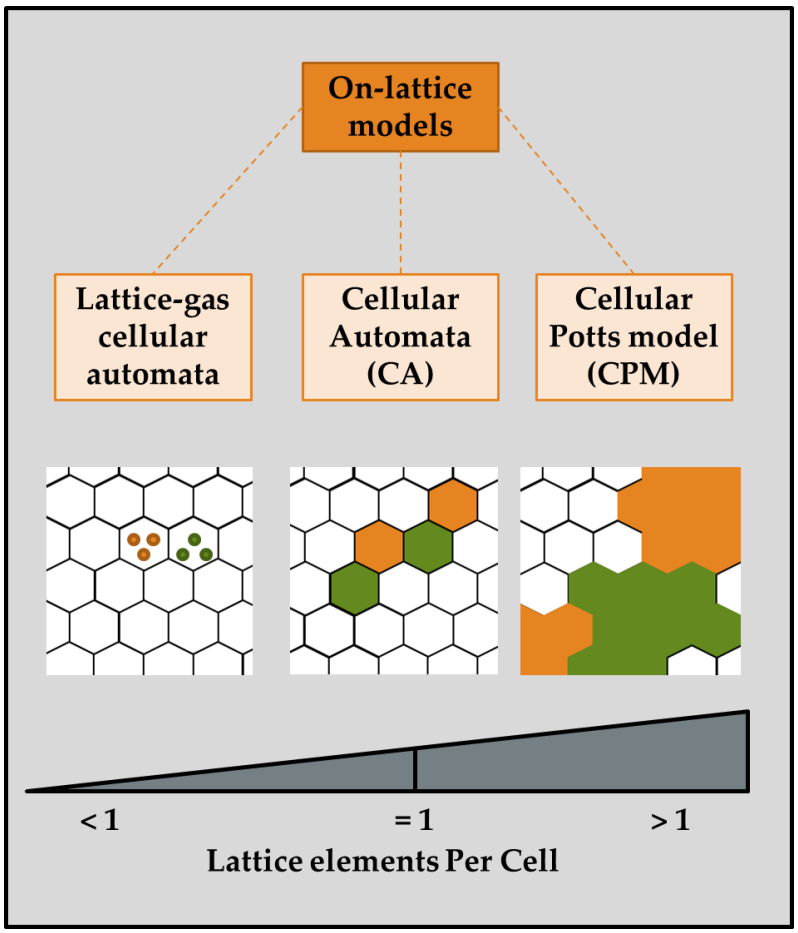

Figure 1.3 A schematic classification of on-lattice models

1.3 Human induced pluripotent stem cells

For decades, stem cells have been used in regenerative medicine and drug screening due to their capabilities of self-renewal and differentiation into various cell types. Since mouse somatic cells were successfully dedifferentiated into pluripotent state with four transcription factors (Oct4, Sox2, Klf4, and c-Myc) by Takahashi and Yamanaka (2006), induced pluripotent stem cells (iPSCs) have received even more attention. For application and regenerative medicine, since iPSCs are developed from a patient's own somatic cells, it helps to avoid any immunogenic responses as well as controversial use of embryos (Takahashi et al. 2007, Yamanaka 2012). Many researches have demonstrated that iPSCs show remarkable similarities to embryonic stem cells (ESCs) in both cell morphology and functionality including

pluripotency and viable chimera formation (Wernig et al. 2007, Maherali et al. 2007). Therefore, it was believed that human iPSCs (hiPSCs) can be an infinite cell source for regenerative medicine.

Bioprocessing of hiPSCs comprises some steps including isolation, derivation, large-scale expansion, differentiation, purification, storage, and distribution of final products (Wang et al. 2014). Cells from donors are collected and reprogrammed into hiPSCs by transcription factors. Then, hiPSCs are expanded and differentiated into desired target cells. Finally, the produced cells are purified before distributed for different aims. In the expansion step, maintenance of the undifferentiated state of hiPSCs is important since the homogeneity of cell pluripotency will ensure the success of differentiation step. Conventionally, to maintain the pluripotency of hiPSCs, cells are cultured with feeder cells that support hiPSC proliferation and adhesion via supplementation of growth factors and extracellular matrix (Saxena et al.2008, Villa-Diaz et al. 2013). Two most popular feeder cell types are mouse embryonic fibroblasts (MEFs) and SNL which is a mouse fibroblast STO cell line transformed with neomycin resistance genes and murine leukaemic inhibitory factor (LIF). They are believed to be different in their potential for maintenance of undifferentiated state. In culture with feeder cells, hiPSCs grow as monolayer colonies and sustain the undifferentiated state. Maintaining the undifferentiated state of hiPSCs remains challenging during the expansion step. Previously, the deviation from the undifferentiated state of hiPSCs in culture with feeder cells has been reported with changes in cell morphology from a small cobblestone-like shape to a large flattened shape (Takahashi and Yamanaka 2006, Takahashi et al. 2009, Kim et al. 2014). This unintentional loss of pluripotency leads to heterogeneous cell population that makes it difficult for long-term maintenance and direct differentiation. In 2014, Kim et al. reported two different patterns of deviation from the undifferentiated state in hiPSC colonies in culture with SNL and MEF feeder cells (**Fig. 1.4**). The deviation from the undifferentiated state of hiPSCs in culture

with SNL feeder cells occurred spontaneously at the central region of colony and was dependent on colony size. On the other hand, the deviation from the undifferentiated state of hiPSCs occurred randomly at the peripheral region of colony and was independent on colony size in culture with MEF feeder cells. At the central regions of colonies, steady decrease of cell migration, partial detachment of cells with disruption of integrin mediated cell-substrate interaction, and morphological changes accompanying cell apoptosis were observed with increasing population density. At the peripheral regions of colonies, loss of E-cadherin mediated cell-cell interaction was found. After all, they suggested that the most important factor for occurrence of hiPSC deviations was cell migration which closely related to cell interactions and morphology.

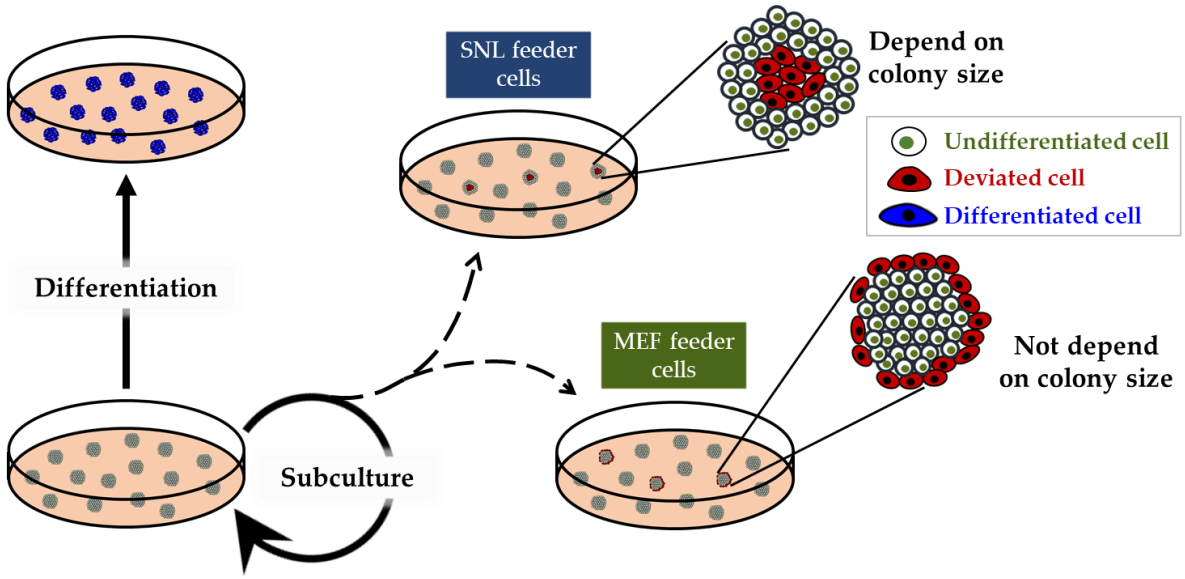

Figure 1.4 Deviation from the undifferentiated state of hiPSCs in culture with SNL and MEF feeder cells (Kim et al. 2014)

1.4 Effect of cell-cell interaction, cell-substrate interaction, and cell migration on hiPSCs

Many researchers have attempted to mimic stem cell niche by designing microenvironments in order to control stem cell fate (Metallo et al. 2007, Lutolf et al. 2009). For that purpose,

understanding how cells interact with their neighboring cells and substrate is necessary. In case of pluripotent stem cells, it becomes even more important since cadherin-mediated cell-cell interaction and integrin-mediated cell-substrate interaction are known to influence cell fate (Metallo et al. 2007, Li et al. 2010, Xu et al. 2010). They both assemble large intracellular protein complexes via their cytoplasmic domains which regulate cell behavior through modulation of signaling networks. For survival and self-renewal of pluripotent stem cells, it was reported that the interplay between Rap1 and E-cadherin along the endocytic recycling pathway (Li et al. 2010), influencing the Oct3/4 and Nanog genes expression by E-cadherin (Metallo et al. 2007), and modulation of PI3K-Akt pathway which inhibits cell death (Paling et al. 2004, Armstrong et al. 2006, Xu et al. 2010) via integrin-mediated cell-substrate interaction played important roles. Also, the down-regulation of E-cadherin was proved to stimulates Caspase-3 and suppress *Bcl-XL* gene that led to increase level of cell death (Watanabe et al. 2007, Ohgushi et al. 2011). Furthermore, it was found that long-term Wnt activation promoted cell differentiation through β-catenin-induced upregulation of *Slug* (Huang et al. 2014). Besides, regulation of cell migration is also one of promising strategies to control cell fate. During cell migration, cadherin-mediated cell-cell interaction and integrin-mediated cell-substrate interaction are continuously broken and reformed. This dynamic of cell interactions triggers a cascade of cell events that starts with the activation of Rho family GTPase (Arthur et al. 2002). In 2012, Khatau et al. showed that cell nucleus responds to cell migration that leads to change in gene regulation and nuclear mechanical properties.

Therefore, the possible mechanisms for controlling cell fate decision by influencing the balance between cell-cell, cell-substrate interactions via altered cell migration have been addressed recently (Kim and Kino-oka 2014a, Kim and Kino-oka 2015, Shuzui et al. 2019b). In culture on dendrimer surface, it was shown that appropriate cell migration leads to formation of hiPSC colonies. While faster cell migration induced differentiation toward cells of early

mesoderm (Kim and Kino-oka 2014b). In culture with feeder cells, cell migration rate at the central and peripheral region of colony before the occurrence of deviation was measured. The analyzed results indicated that there were more slow or fast migrating cells at the central or peripheral region, respectively, in colonies with deviated cells than in colonies with undifferentiated cells (Shuzui et al. 2019a). Later, when migration of hiPSCs were accelerated via alteration of cell-cell interaction, the deviation from the undifferentiated state at the central region of colonies cultured with SNL feeder cells was avoided (Shuzui et al. 2019b).

1.5 Adhesion energy

The adhesion energy of a hiPSC comes from bonds formed between that cell and it's adjacent cells or substrates and are mainly determined by adhesion molecules E-cadherin and integrin, respectively. Main functions of adhesion energy are controlling the adhesive strength and morphology of the cell contact (Maitre and Heisenberg 2011). Together with cortical tension, adhesion energy is a key parameter indicating the interaction between cells and their surrounding environment. The finding about relation between the force required to separate contacting cells and the number of E-cadherin molecules in the cells (Chu et al. 2004, Arboleda-Estudillo et al. 2010) suggested that the number of E-cadherin affected adhesion energy between cells. Many strategies and techniques have been used to estimate the adhesion energy such as bioforce probe, atomic force microscopy, and dual pipette assay (Jegou et al. 2008, Moreno-Cencerrado et al. 2017, Daoudi et al. 2004). But it is noteworthy that E-cadherin does not only bind to other cadherin via the extracellular domain but also bind to the cytoskeleton via the intracellular domain (Nagafuchi and Takeichi 1988). Therefore, the energy measured by detaching cells might be different from the adhesion energy which indicates the binding strength of E-cadherin at the extracellular domain. Similarly, detachment energy is also usually used to quantify adhesion energy between cell and extracellular matrix. Li et al.

(2003) defined the detachment energy as the work done to break the $\alpha_5\beta_1$ bonds and deform the cell during the detachment process that depended on the number of integrin-fibronectin complexes formed. In summary, in case of hiPSCs, cell-cell adhesion energy and cell-substrate adhesion energy are the energies required to detach E-cadherin/E-cadherin bonding between two cells and integrin/substrate bonding of one cell. These energies are suggested to depend on the number of E-cadherin and integrin at binding sites. Physically, these energies are considered as potential energy while kinetic energy is the energy of movement.

1.6 Features of our model

Two main features of our model are the multi-scalability and the modularity. Multiscale modeling is a type of modelling in which different spatiotemporal scales of a system are described and linked together. It allow us to express the dynamic exchange of information across scales of a system (Cilfone et al. 2014). A multiscale model can be built by either bottom-up or top-down approach (Meier-Schellersheim et al. 2009). In the top-down approach, the modelers start from the observed features on a highest level of a system, then the mechanisms on lower levels are inferred. For a biological system, this approach may go from society to body, organ, tissue, cell, organelle, protein, to gene (Qu et al. 2011). Even though this type of modeling is relatively simple, it's variables and parameters are mainly phenomenological and do not directly connect with actual physiological parameters (Qu et al. 2011). In contrast, in the bottom-up approach, the behaviors of a system on higher levels are derived from the lower scales after the individual elements and their interactions are described. The greatest advantage of this modeling approach is that it is suitable for systems with massive interacting elements (Qu et al. 2011). However, it is usually too complicated and computationally costly. In this study, our interested phenomenon is the deviation from the undifferentiated state of hiPSCs in colonies that requires spatiotemporal analysis at many

scales. Therefore, the multiscale model was developed which described from single cell level (microscale), colony level (mesoscale), to culture level (macroscale) (**Fig. 1.5**). On the lowest level, each cell was expressed by many cell behaviors and could be analyzed separately to understand the deviation trigger. In this level, the heterogeneity between neighboring cells was expressed by the model. On the next level, cell colonies which were made up of connected cells were maintained and expanded by fundamental cell behaviors including cell division, cell migration, and cell connections. Since the spatial heterogeneity in each colony was realized, spatiotemporal frequency for occurrence of deviation in colony could be analyzed. Lastly, the culture level was obtained by the heterogeneity between colonies in the culture vessel. On this level, the frequency of deviation trigger in whole culture was concerned.

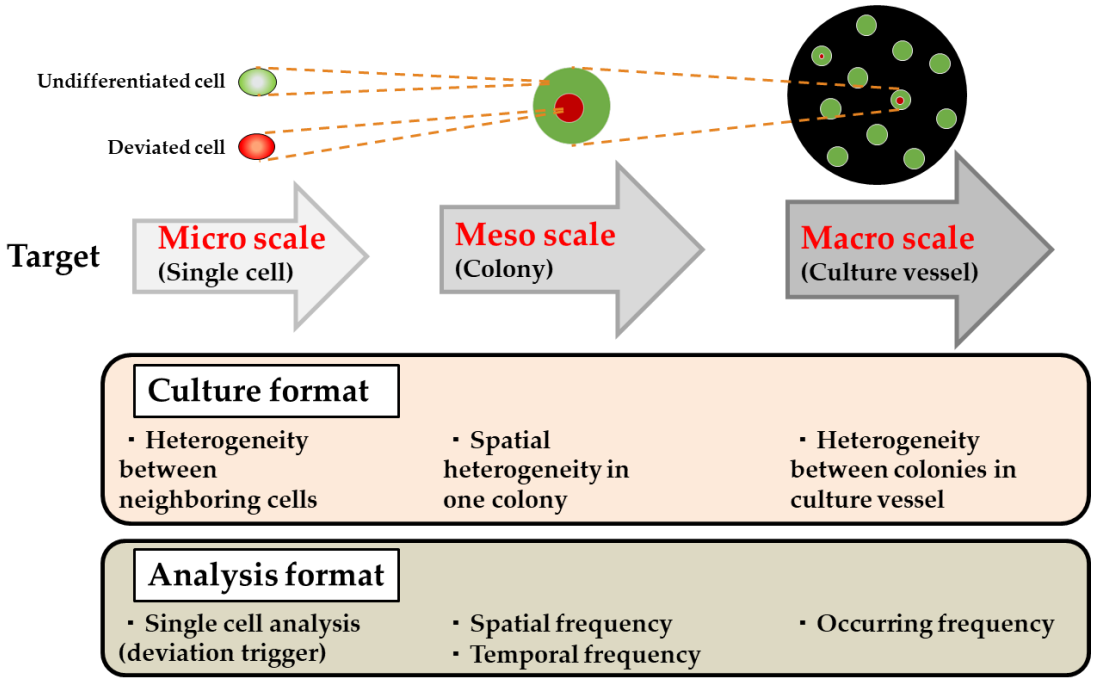

Figure 1.5 Multi-scalability of the developed kinetic model for hiPSC culture in this study

The second key feature of our model is the modularity. Modular modeling is a type of modeling where interchangeable components (modules) are used. According to McClelland and Rumelhart (1995) and Baldwin and Clark (2000), a module is a unit in a system that interacts with other modules in the system and accessible via interface. In the biological field, this modeling method has been mainly applied in system biology (Saez-Rodriguez et al. 2005,

Marchisio et al. 2013, Avsec et al. 2018, Cheng et al. 2019). In this study, with the idea of building a modular system for hiPSC culture, each cell behavior as well as culture operation were modelled separately in different modules (**Fig. 1.6**). The model was built as "plug-and-play" form where the main model could be pre-defined by choosing modules from the user interface. Many modules expressing cell behaviors (e. g. cell division, cell migration, cell connections), culture operations (e. g. culture seeding), culture environments (e. g. culture space and time), and outputs (e. g. movement rate calculation) have been built after several research directions that made up a large module warehouse (**Fig. 1.7**). Current modules in warehouse can be modified or new modules can be added according to updated rules or demands. The modular model helps to express the variety of cell types with different needs. For a certain culture system, suitable modules can be selected from module warehouse, new modules can be added if necessary and unused modules can be removed (**Fig. 1.8**). Therefore, the model gives access to not only culture of hiPSCs with feeder cells in current study but also other related systems in future. Advantages of modular biological models including component reuse and model integration for different use cases have been addressed previously by Petersen et al. (2014). They believed that modularizations methods would accelerate the pace of biomedical research.

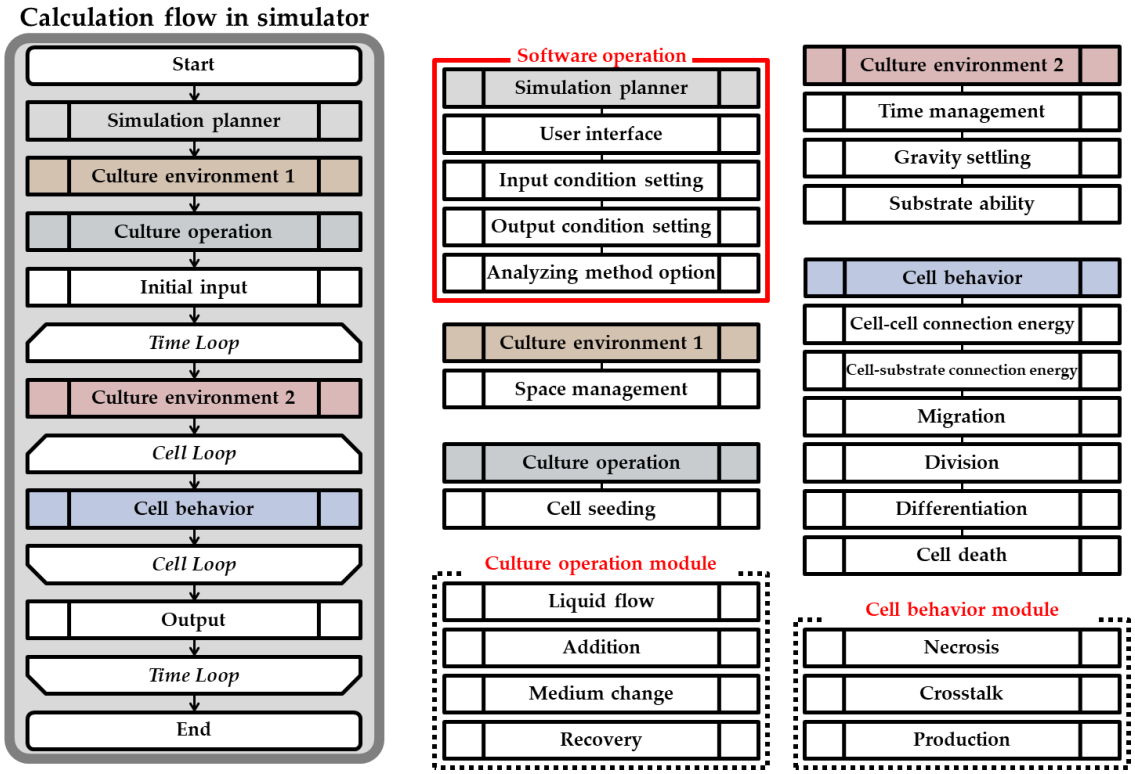

Figure 1.6 Schematic drawing of idea of modular system for modelling

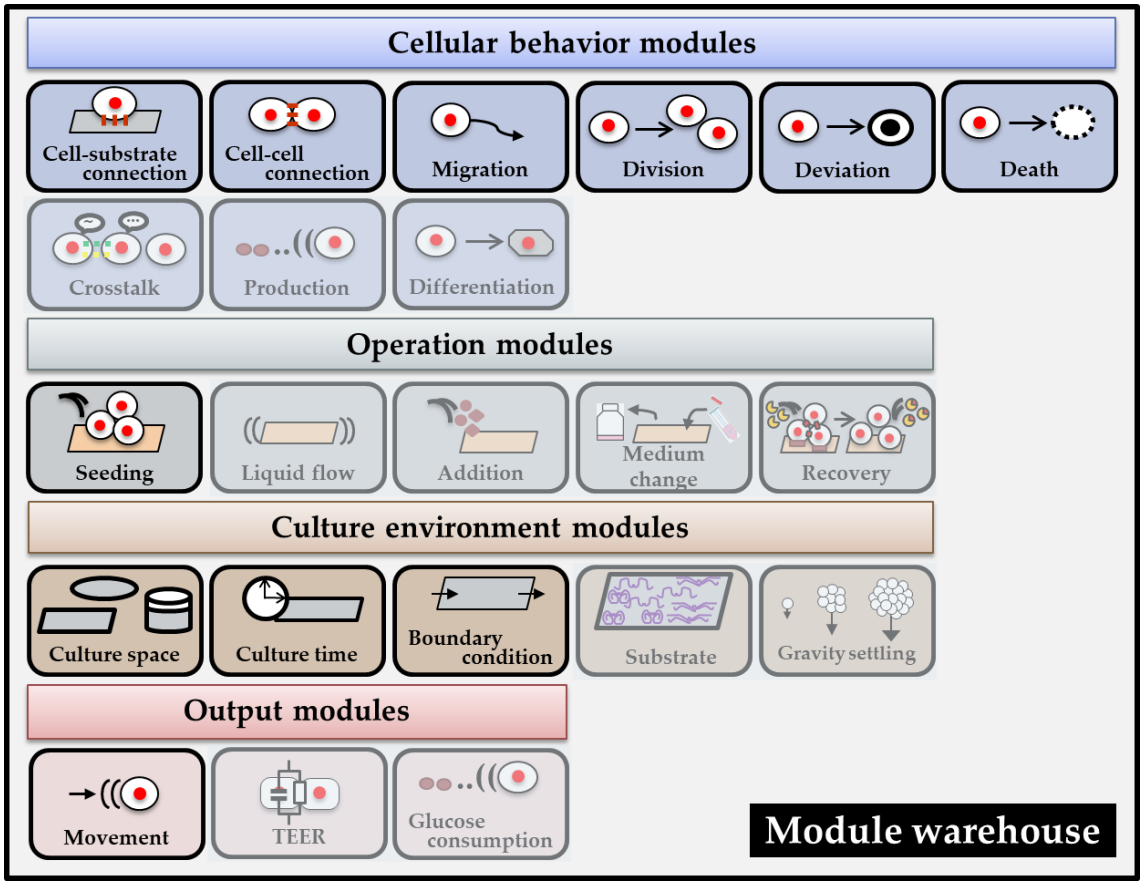

Figure 1.7 Schematic drawing of examples of modules in module warehouse

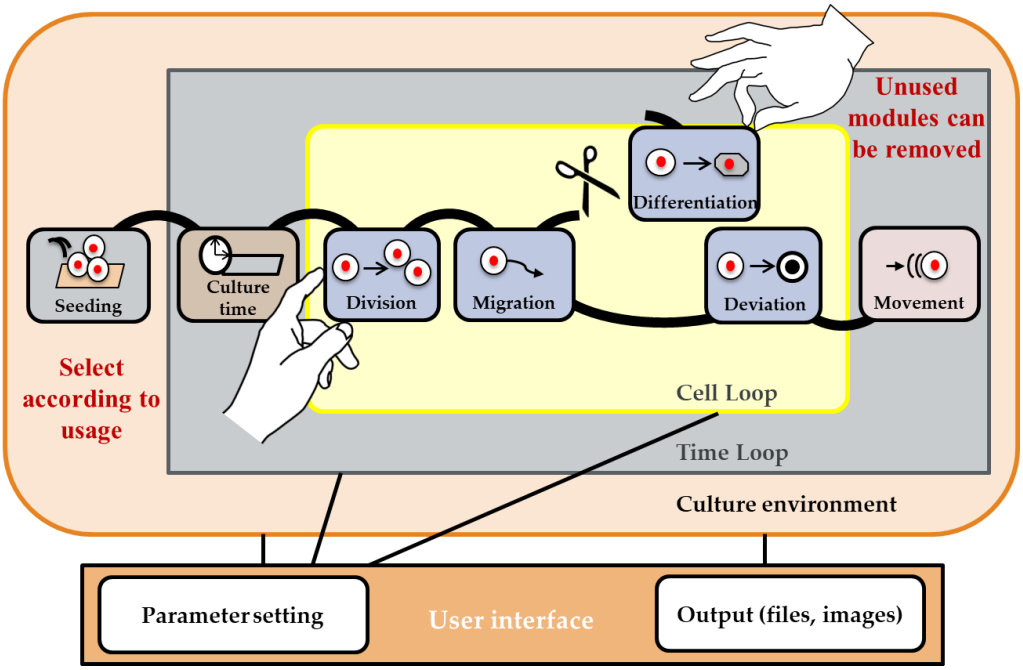

Figure 1.8 Schematic drawing of process for model pre-defining for a certain culture system

1.7 Strategies and objectives of this study

With promising roles in regenerative medicine and drug screening, how to assure hiPSC quality throughout the cell production process is crucial mission. Focusing on culture of hiPSCs with feeder cell layers, previous studies have pointed out that anomalous cell migration at the central and peripheral region of colony is a possible trigger for the loss of hiPSC pluripotency (Shuzui et al. 2019a). However, many questions have been still remained after all efforts of *in vitro* study due to technical limitation that raises the need of kinetic modelling. My strategy was developing a kinetic model which can help to understand how often deviation occurred in culture, when cells deviated, and what regions of a colony were subject to deviation. Then, I firstly used the developed model to understand what caused the heterogeneity of cell migration where cells at the peripheral region of colony have higher migration rate then cells at the central region of colony (Chapter 2). From *in silico* analysis and previous *in vitro* hypothesis about the deviation from the undifferentiated state of hiPSCs, I established *in silico* hypothesis about deviation from the undifferentiated state of hiPSCs (Chapter 3). The model was validated by

comparing *in silico* output and *in vitro* data. With the validated model, I expected to be able to deeply understand the trigger for the deviation from the undifferentiated state of hiPSCs cultured on feeder cells.

Chapter 2 Understanding the spatial heterogeneity of cell migration in colony

2.1 Introduction

For more efficient stem cell engineering, there is a need to utilize kinetic model instead of only relying on the empirical knowledge of professionals. It helps to manage processes non-invasively, control stem cell quality, elucidate the mechanism of the phenomenon of interest, and predict the outcome. In many cases, kinetic model has been successfully used to predict stem cell fate as well provide insights into the mechanism underlying some processes (Viswanathan and Zandstra 2003, MacArthur et al. 2009, Herberg and Roeder 2015).

Heterogeneity of propagated stem cell populations is one of challenges in stem cell processing that need to be overcome prior to their routine therapeutic application (Chowdhury et al. 2010, Serra et al. 2012, Chen et al. 2014). Understanding underlying mechanisms of the heterogeneity is the core issue to keep the cell population homogeneous. Previously, some reports have shown the heterogeneity of stem cell colonies or aggregation with spatial heterogeneity in cell state (Bratt-Leau et al. 2009, Kim et al. 2014, Rosowski et al. 2015). Kim et al. (2014) reported the heterogeneity in cell quality where deviated cells were found at the central and peripheral region of colony. Concerning this phenomenon, Shuzui et al. (2019a) analyzed *in vitro* cell migration rate and showed that cell migration rate was higher at the peripheral region of colony than at the central region of colony. Furthermore, they suggested that the anomalous cell migration at those areas are triggers for the deviation from the undifferentiated state of hiPSCs. This *in vitro* cell migration rate is resulted from exchange between neighboring cells and displacement caused by cell division. Due to technical limitation, it is difficult to understand effect of each of these two factors on the overall *in vitro* cell migration rate.

In this chapter, my objective is developing a kinetic model based on cellular automaton approach to understand the key factor that leads to the heterogeneity of cell migration in hiPSC

colonies. The contribution of cell exchange and cell division needs to be clearly understood prior to considering cell migration as triggers for deviation from the undifferentiated state of hiPSCs in culture with feeder cells.

2.2 Materials and Methods

2.2.1 Culture of hiPSCs

Maintenance of hiPSCs (clone Tic, JCRB1331) were performed in 55-cm^2 dishes (Corning Costar, Cambridge, MA) with feeder cells SNL 76/7 (European Collection of Cell Cultures, Salisbury, UK) or mouse embryonic fibroblasts (MEFs) (ReproCELL Inc., Tokyo, Japan) at 37°C, 5% CO_2. The surface was coated with 0.1% gelatin and the medium ReproStem (ReproCELL Inc.) containing 5 ng/mL basic fibroblast growth factor was used. Subculture of hiPSCs were performed every 5 days. More details about *in vitro* culture are mentioned in previous paper (Shuzui et al. 2019a).

A two-dimensional CA which consists an array of cubes having a finite number of states and can change their states at every time step was used for *in silico* culture. Depending on the purpose of each experiment, the simulation was initiated by seeding single or multiple colonies. In seeding process, we assumed that the adhesion time and lag time are negligible and the attachment ratio was assumed to be one. Other assumptions were indicated in previous work (Kagawa and Kino-oka 2016). After that, simulations were executed with four cell behaviors with time t was increased by a time step Δt of 0.1 h. LabVIEW (National Instruments Corp., Austin, Texas, USA) environment on the commercially available workstation (Precision T7500 workstation, Dell Inc., Round Rock, Texas, USA) was used to execute *in silico* culture. In this model, we assumed that the effects of feeder cells on hiPSCs as physical barriers could be negligible and did not include feeder cells in the model. SNL and MEF feeder cells were believed to help hiPSCs attach and maintain their undifferentiated state via various growth

factors and extracellular matrix components. Therefore, the effects of SNL and MEF feeder cells were realized by different parameter values related to cell growth and cell connections.

2.2.2 Analysis of movement rate of hiPSCs in colony

Movement rates of individual cells in a colony was calculated by the displacement of a cell divided by the duration of the movement time:

$$V_c = \frac{\sqrt{(X_t - X_{t-dt})^2 + (Y_t - Y_{t-dt})^2}}{dt} l_c \quad (1)$$

where (X_t, Y_t) and (X_{t-dt}, Y_{t-dt}) are coordinates of a cell at culture time t h and $(t - dt)$ h; l_c is the length of the unit cube. t and dt were determined to be 54 h and 6 h, respectively, to estimate cell migration-related parameters.

The average movement rate against the distance from the center of the colony $\overline{V_R}$ was calculated by taking an average of cell movement rate V_c of all cells at every 100 μm from the center of the colony at t = 50 h, 90 h, 128 h, and dt = 6 h.

Average cell movement rate, V_M, is the average of cell movement rate V_c of all cells at the central and peripheral regions of the colony, which were determined as the 4 inner- and outermost cell layers of the colony, respectively. To investigate the relationship between pushing frequency and average cell movement rate, V_c was estimated at t = 72 h, 96 h, 120 h, 144 h, and dt = 24 h.

2.2.3 Analysis of cell movement rate toward the outside of colony, $V_c \cos\theta$

The central and peripheral regions of the colony were determined as the 4 inner- and outermost cell layers of the colony, respectively, at t = 48 h. The movement rate toward the outside of colony, $V_c \cos\theta$, of cells at the central and peripheral regions of the colony were analyzed from t = 48 h to t = 54 h. Angle θ was determined by $180° - \widehat{OA_cB_c}$ where O is the center of the

colony, A_c and B_c are positions of cell c at t = 48 h and t = 54 h, respectively. Inward movement to the center of colony was indicated by negative $V_c \cos\theta$. In contrast, outward movement to the outside of colony was indicated by non-negative values. Frequencies of cells with different value ranges of $V_c \cos\theta$ were analyzed from three single *in silico* colonies.

2.2.4 Tracking cell movement *in silico*

At t = 24 h, positions of three cells at the central region and at the edge of colony cultured on MEF feeder cells were tracked every 30 min for 120 h. Tracked cells at the central region were marked in yellow and those at the edge of the colony were marked red. Non-tracked cells in the colony were marked in blue.

2.2.5 Calculation of average frequency of being pushed

Average frequency of being pushed is the average of the frequency that a cell was pushed out due to the division of other cells. The frequency of one cell being pushed P_c (times/h) was calculated as follows:

$$P_c = \frac{\text{times being pushed from } (t - dt) \text{ to } t}{dt} \quad (2)$$

where t = 72 h, 96 h, 120 h, 144 h, dt = 24 h.

2.2.6 Fitting method

The least-squares method was used to find the best fit values of the number of cell layers for occurrence of contact inhibition (N_c), free migration rate ($V_{m,free}$), ratio of energy for a cell-cell connection (ε_{cc}), ratio of energy for a cell-substrate connection (ε_{cs}).

2.2.8 Statistical analysis

To validate simulated results of colony size distribution in the culture vessel against experimental data at 24 h and 120 h after seeding, Mann–Whitney U test was used at a significance level of 0.05 (number of colonies: $n > 50$).

2.3 Results

2.3.1 Model development

Rules of cell connection

Each cell can form cell-cell connections with other cells or cell-substrate connections with the substrate via cadherin- and integrin- mediated interactions. However, modeling these interactions at molecular level is a challenging work. Therefore, we came up with an idea of focusing on the energy that a cell utilizes to form cell-cell and cell-substrate connections. Cell-cell and cell-substrate connection energies are denoted as E_{cc} and E_{cs}, respectively. The distance between them should be small enough for a cell to make a connection with another cell or the substrate cube. Here, I assumed that the unit cube could make a connection with the target cell when the distance between the center of the cell or substrate unit cube and that of the target cell cube was not more than $\sqrt{2}l_c$ (**Fig. 2.1**). When cell i and cell j made a connection, the connection energy between them was given by $E_{\mathrm{cc}} = \min(E_{\mathrm{cc},i}, E_{\mathrm{cc},j})$. The connection energy between cell c and the substrate is given by $E_{\mathrm{cs}} = E_{\mathrm{cs},c}$.

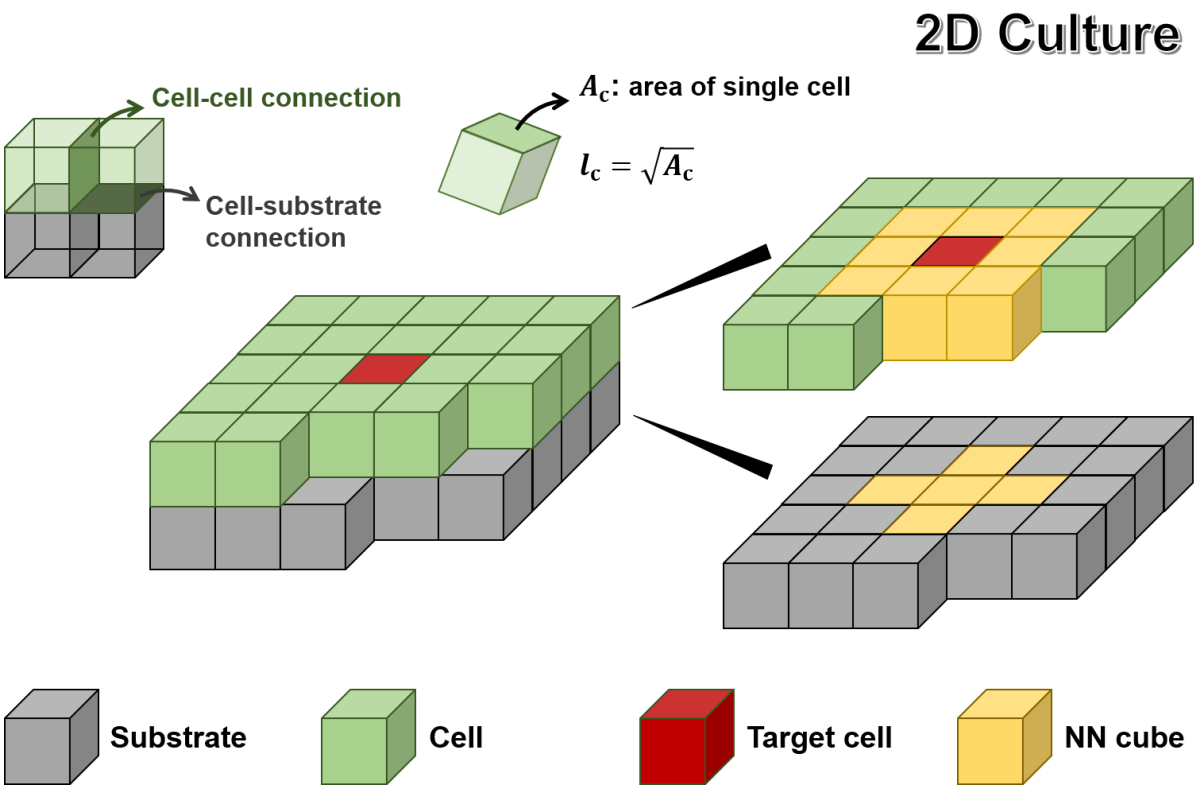

Figure 2.1 Schematic drawing of our model that describes the definition of cell size, cell connections, and NN cubes surrounding the target cell in case each cell is presented by a cube.

Rules of cell migration

In vitro cell migration is a complex process which involves drastic changes in the cellular cytoskeleton and the dynamic of cell interactions. Therefore, this process was simplified as follows: a cell uses energy to break and form cell-cell and cell-substrate connections immediately, the remaining energy will be used for cell migration. Cells can choose one of eight distinct directions denoted by the variable dir to migrate to. When cell c migrates to the direction dir with the rate of $V_{\mathrm{m},c}$, the variable $t_{\mathrm{m},c}$, a waiting time for the next migration, is updated as $t_{\mathrm{m},c} = l \cdot V_{\mathrm{m},c}^{-1}$, where l is the migration distance. The waiting time $t_{\mathrm{m},c}$ decreases by Δt for each time step. If the waiting time is bigger than zero ($t_{\mathrm{m},c} > 0$), then cell c does not actively migrate, but still can be passively exchanged (passive migration) with the NN cells whose waiting times are less than zero.

If the waiting time of cell c becomes equal or less than zero ($t_{\mathrm{m},c} \leq 0$), the direction dir and the rate $V_{\mathrm{m},c}$ of migration are decided as follows: first, the direction dir is determined stochastically based on the probability $Pr_{\mathrm{m},dir}$ which is given by the normalized quantity $p_{\mathrm{m},dir}$. This normalized quantity is proportional to (i) the term relating to the connection energy between the target cell cube and the other cell and/or substrate cubes reduced by the migration ($R_{\mathrm{m},dir}$), (ii) the weight for randomly selecting a space (Ω_{dir}) (Kino-oka et al. 2000), and (iii) the possibility of displacement ($H_{\mathrm{m},dir} = 0$ or 1).

A weight for occurrence of migration to the direction dir was defined by the following equation:

$$R_{\mathrm{m},dir} = 1 - \frac{E_{\mathrm{B},dir}}{E_{\mathrm{A}}} \tag{3}$$

where E_{A} and $E_{\mathrm{B},dir}$ are the total connection energy formed by the target cell before migration and the total reducing connection energy due to migration to the direction dir, respectively.

E_{A} is defined as follows:

$$E_{\mathrm{A}} = \sum_{dir=0}^{N_{\mathrm{nn}}-1} E_{c,dir} \tag{4}$$

where E_c is either E_{cc} or E_{cs}, N_{nn} is the number of NN cubes (N_{nn} = 13 in 2D culture (**Fig. 1.5**).

$E_{\mathrm{B},dir}$ was defined by equation (3) and must not exceed the maximum migration energy E_{max}.

$$E_{\mathrm{B},dir} = \sum_{dir=0}^{N_{\mathrm{nn}}-1} \Delta E(d; dir) \tag{5}$$

where $\Delta E(d; dir)$ is the reduced amount of connection energy between the target cell and the nearest neighbor cubes when the target cell moves in the direction dir.

Cells cannot migrate to a position where they cannot make any connections with other cells or the substrate. The migration can occur only when the target cell can make a connection in new destination with at least one other cell or substrate cube. Cell migration does not occur once this condition is violated and the possibility of displacement is defined to be zero: $H_{\mathrm{m},dir} = 0$. Otherwise, $H_{\mathrm{m},dir} = 1$ is given.

The probability for selecting dir as the direction of migration $p_{\mathrm{m},dir}$ when there is no other cells neighboring a target cell is given by

$$p_{\mathrm{m},dir} = \frac{R_{\mathrm{m},dir}\,\Omega_{dir}\,H_{\mathrm{m},dir}}{\sum_{dir'=0}^{N_{\mathrm{nn}}-1}(R_{\mathrm{m},dir'}\,\Omega_{dir'}\,H_{\mathrm{m},dir'})}. \tag{6}$$

If the denominator becomes zero, there is no need to calculate the probability because the target cell cannot migrate in any direction.

The probability for selecting dir as the direction of migration in general is given by

$$Pr_{\mathrm{m},dir} = \frac{(p_{\mathrm{m},dir})_{\mathrm{T}}(p_{\mathrm{m},\widetilde{dir}})_{\mathrm{D}}}{\sum_{dir'=0}^{N_{\mathrm{nn}}-1}(p_{\mathrm{m},dir'})_{\mathrm{T}}(p_{\mathrm{m},\widetilde{dir'}})_{\mathrm{D}}} \tag{7}$$

where $(p_{\mathrm{m},dir})_{\mathrm{T}}$ represents the probability that the target cell selects dir as the direction of migration as if there are no other neighboring cells, and $(p_{\mathrm{m},\widetilde{dir}})_{\mathrm{D}}$ represents the probability that another cell exists at the destination selects the direction opposite to dir (designated as $\widetilde{dir}$). If there is no other cell at the destination, then we substitute 1 for $(p_{\mathrm{m},\widetilde{dir}})_{\mathrm{D}}$. In this case, we have $Pr_{\mathrm{m},dir} = p_{\mathrm{m},dir}$.

Assumed that cell has a maximum energy that can be used for the migration ($E_{\max}$)

$$E_{\max} = \frac{1}{2} m_c V_{\mathrm{m,free}}^2 \tag{8}$$

where $V_{\mathrm{m,free}}$ represents the migration rate when no connection is broken and m_c is the mass of cell c.

Then, when it migrates in the direction dir, the total reducing connection energy $E_{\mathrm{B},dir}$ is subtracted from $E_{\max}$ is used for the migration:

$$\frac{1}{2}m_c V_{\mathrm{m},c}^2 = E_{\max} - E_{\mathrm{B}} \tag{9}$$

where $V_{\mathrm{m},c}$ is the cell migration rate

Using the two equations above, we obtained the following relationship:

$$V_{\mathrm{m},c} = V_{\mathrm{m,free}}\sqrt{1 - E_{\mathrm{B}}/E_{\max}} = V_{\mathrm{m,free}}\sqrt{1 - i\varepsilon_{\mathrm{cc}} - j\varepsilon_{\mathrm{cs}}} \tag{10}$$

where $\varepsilon_{\mathrm{cc}}$ ($\varepsilon_{\mathrm{cc}} = E_{\mathrm{cc}}/E_{\max}$) and $\varepsilon_{\mathrm{cs}}$ ($\varepsilon_{\mathrm{cs}} = E_{\mathrm{cs}}/E_{\max}$) are ratio of energy for cell-cell and cell-substrate connection in maximum energy, and i and j are the number of broken cell-cell and cell-substrate connections, respectively.

Rules of cell division

After sufficiently preparing genetic material and mass in each cell cycle, a proliferating cell divides into two identical daughter cells that continue to grow to their full size. In this model, only the duplication of one mother cell into two identical daughter cells is described and the change in cell size is ignored. Proliferating cells divide every generation time t_{g} which is a stochastic variable given randomly from $[0.9\bar{t_{\mathrm{g}}}, 1.1\bar{t_{\mathrm{g}}}]$ (uniform distribution) at the beginning of each cell cycle. The parameter $\bar{t_{\mathrm{g}}}$ is the mean generation time which is estimated by $\ln(2)/\mu_{\mathrm{p}}$. μ_{p} is a specific growth rate of *in vitro* cell culture. Each cell has a waiting time for the next division $t_{\mathrm{d},c}$ which equals t_{g} at the time of cell birth and is decreased every time step. When $t_{\mathrm{d},c}$ of a proliferating cell is less than zero, this cell can divide and update $t_{\mathrm{d},c}$ as $t_{\mathrm{d},c} = t_{\mathrm{d},c} + t_{\mathrm{g}}$. If there are vacant NN cubes, the mother cell puts its daughter cell on one of the vacant NN cubes stochastically as described previously (Kino-oka et al. 2000). Otherwise, it first selects one of the closest vacant cubes, then one of the NN cells of the selected vacant cube is moved to that cube. The procedure is repeated until the mother cell has a vacant NN cube to place the daughter cell in.

Rules of cell quiescence

We assumed that whenever there is no vacant space in the distance N_{c} from the center of a cell,

it enters a quiescent state and the waiting time for the next division does not decrease for each time step. Whenever a vacant space appears at the distance N_c from the center of a quiescent cell, it returns to a proliferating state at the next time step.

2.3.2 Estimation of model parameter values

The length of a side of the unit cube l_c was estimated from the averaged cell area A_c which equaled 329 μm^2 and 426 μm^2 in cultures of hiPSCs on SNL and MEF feeder cells, respectively. l_c were 18.1 μm and 20.6 μm for cells cultured on SNL and MEF feeder cells, respectively. Mean generation time, $\overline{t_g}$, was calculated by $\ln(2)$ divided by the specific growth rate of hiPSCs in culture and equaled 15.8 h and 21.5 h in culture on SNL and MEF feeder cells, respectively.

The number of cell layers for the occurrence of contact inhibition N_c was estimated by fitting to the experimental growth profile of undifferentiated colonies (**Fig. 2.2**). Single *in silico* colonies were seeded with radius of 9 and 7 cell layers in culture on SNL and MEF feeder cells, respectively. Initial colony sizes were determined as the average size of *in vitro* colonies at 24 h from previous paper (Kim et al 2014). The value of N_c was changed in the range of [1, 10] (cell layer) and its best fit values were 7 cell layers (coefficient of determination R^2 = 0.99) and 8 cell layers (coefficient of determination R^2 = 0.99) in culture on SNL and MEF feeder cells, respectively.

In vitro cell migration rate at the central and peripheral regions of 10 representative colonies in culture on SNL and MEF feeder cells at 48–54 h were used for fitting free migration rate $V_{m,free}$, ratio of cell-cell connection ε_{cc}, and ratio of cell-substrate connection ε_{cs}. *In silico* colonies were seeded with a radius of 10 cell layers until their sizes reached 0.5 mm^2. Then, the movement rates of cells at the central and peripheral regions were calculated. The value of $V_{m,free}$ was changed in the range of [1.0, 15.0] (μm/h), ε_{cc} and ε_{cs} were changed in the range

of [0.05, 0.35] (-). The combination ($V_{\mathrm{m,free}}$, $\varepsilon_{\mathrm{cc}}$, $\varepsilon_{\mathrm{cs}}$) which gave the closest movement rate to the experimental data was determined as (4.0 μm/h, 0.15, 0.05) and (4.0 μm/h, 0.05, 0.15) when cultured on SNL and MEF feeder cells, respectively. *In silico* average movement rate of hiPSCs at the central and peripheral region were 2.9 ± 1.9 μm/h and 5.6 ± 3.3 μm/h or 3.6 ± 2.3 μm/h and 5.6 ± 3.3 μm/h when cultured on SNL or MEF feeder cells, respectively (**Fig. 2.3**). Summarization of parameters values were presented in **Table 1**.

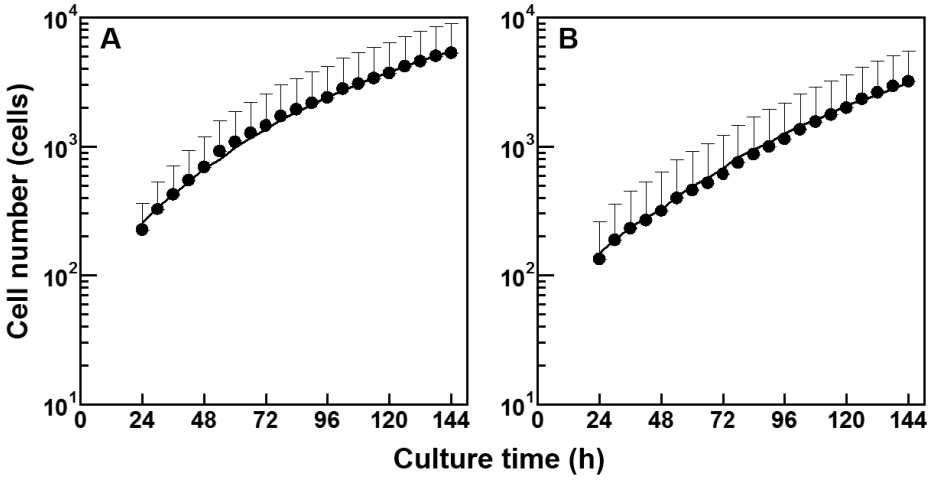

Figure 2.2 Estimation of contact inhibition by fitting to time profiles of hiPSC colonies with undifferentiated cells in cultures on SNL (A) and MEF (B) feeder cells. Closed circle: *in vitro* data; Line: best fit *in silico* data

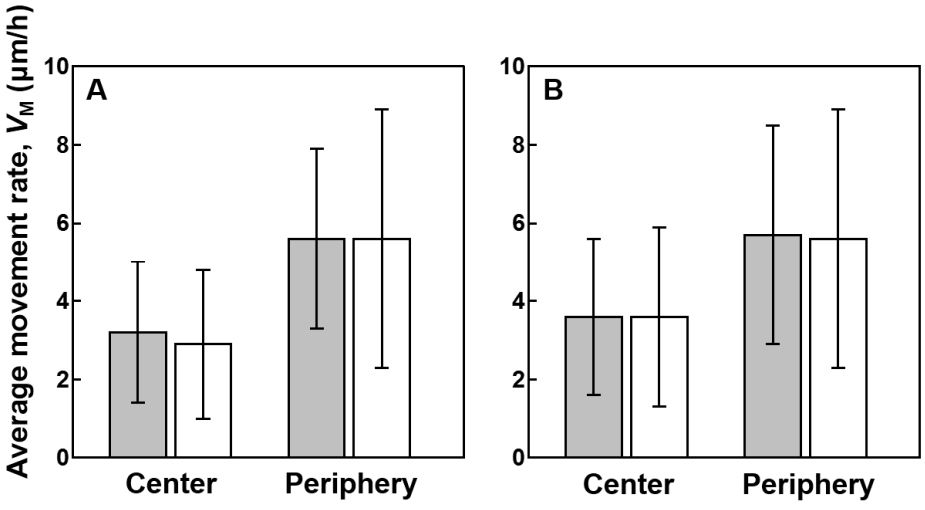

Figure 2.3 Estimation of $V_{\mathrm{m,free}}$, $\varepsilon_{\mathrm{cc}}$, and $\varepsilon_{\mathrm{cs}}$ by fitting to the average movement rate at the central and peripheral regions of hiPSC colonies cultured on SNL (A) and MEF (B) feeder cells. Grey bars: experimental results obtained from 10 colonies. White bars: best fit simulation results obtained by the least-squares method. Standard deviations were calculated from all cells in colonies ($n \geq 300$)

Table 1 *in silico* parameters for undifferentiated cells cultured on SNL and MEF feeder cells

Variable	Symbol	Unit	Value
The length of a side of the unit cube	l_c	μm	18.1 (SNL), 20.6 (MEF)
Mean generation time	$\bar{t}_{\mathrm{g}}$	h	15.8 (SNL), 21.5 (MEF)
The number of cell layers for the occurrence of contact inhibition	N_{c}	cell layer	7 (SNL), 8 (MEF)
Free migration rate	$V_{\mathrm{m,free}}$	μm/h	4.0
Ratio of energy for cell-cell connection	$\varepsilon_{\mathrm{cc}}$	-	0.15 (SNL), 0.05 (MEF)
Ratio of energy for cell-substrate connection	$\varepsilon_{\mathrm{cs}}$	-	0.05 (SNL), 0.15 (MEF)

2.3.3 Validation of the model

After estimating parameter values, we performed *in silico* culture of hiPSCs on SNL and MEF feeder cells for 144 h (Movies S1-2). Position and size of every single colony in *in vitro* culture vessels at t = 24 h were estimated and used as initial seeding conditions for *in silico* culture. *In silico* cell density in culture vessels every 24 h and colony size at t = 120 h were calculated and compared to *in vitro* data. *In silico* growth curves were in good agreement with the *in vitro* data with high coefficients of determination R^2 of 0.94 and 0.97 in culture on SNL and MEF feeder cells, respectively (**Fig. 2.4**). The boxplots in **Fig. 2.5** expressed *in vitro* and *in silico* distributions of colony size in 3 representative culture vessels. These results showed good

agreement between *in vitro* and *in silico* distribution of colony size at t = 24 h and t = 120 h. The Mann–Whitney U test indicated that there was no significant difference in colony size between *in vitro* and *in silico* culture vessels ($P > 0.05$).

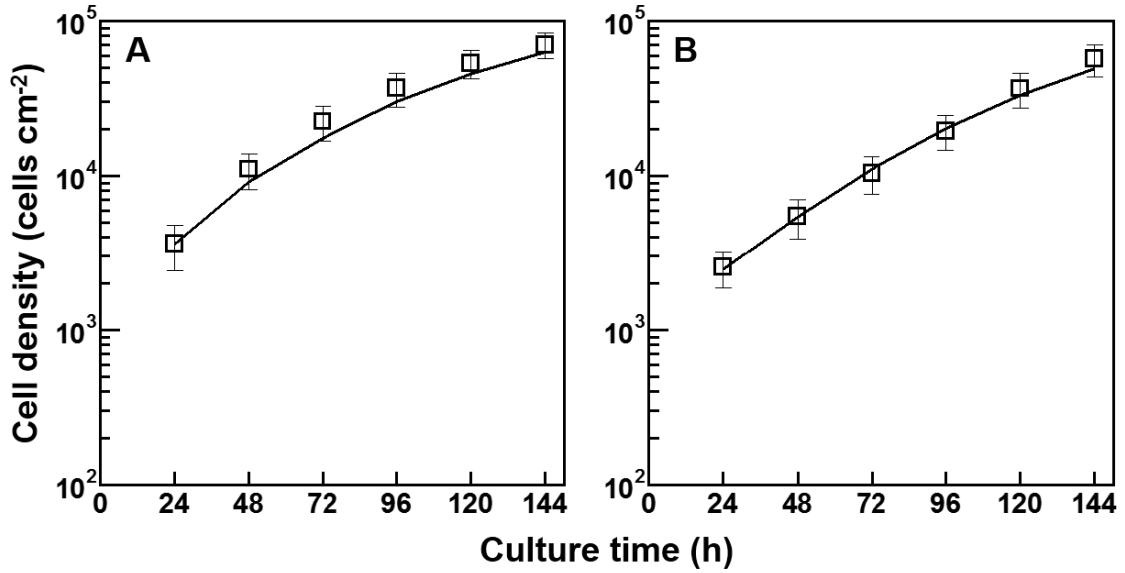

Figure 2.4 Time profiles of hiPSCs in culture wells with only undifferentiated cells cultured on SNL (A) and MEF (B) feeder cells. The data represent analytical results obtained from 3 wells. Open square: *in vitro* data, line: *in silico* data

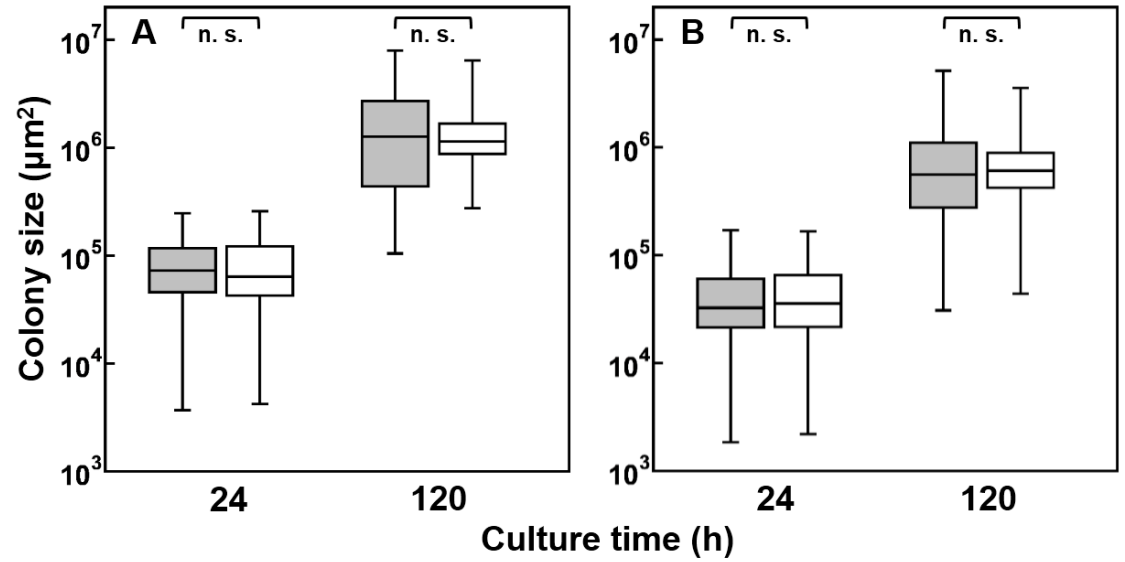

Figure 2.5 Distribution of colony sizes obtained under culture on SNL (A) and MEF (B) feeder cells at 24 h and 120 h after seeding. Grey box: *in vitro* data, white box: *in silico* data. In each

box plot, the central point represents the median, the box gives the interval between the 25% and 75% percentiles, and the whisker indicates the range

For validation of the developed model regarding cell migration behavior in colonies, the cell movement rate toward the outside of colony, $V_c \cos\theta$, of cells at the central and the peripheral regions were examined. *In silico* cells had similar trends of cell movement direction to *in vitro* cells at both regions. Cells moving toward the outside of the colony made up 67% of the central region and 87% at the peripheral region of *in silico* colonies cultured on SNL feeder cells, while those frequencies were 71% and 96%, respectively, for *in vitro* culture (**Fig. 2.6A**). The similar trend was observed in colonies cultured on MEF feeder cells (*in silico*: 65% at the central region and 86% at the peripheral region; *in vitro*: 66% at the central region and 98% at the peripheral region) (**Fig. 2.6B**). Both *in viro* and *in silico* cells moved outward more at the peripheral region of colony than at the central region of colony.

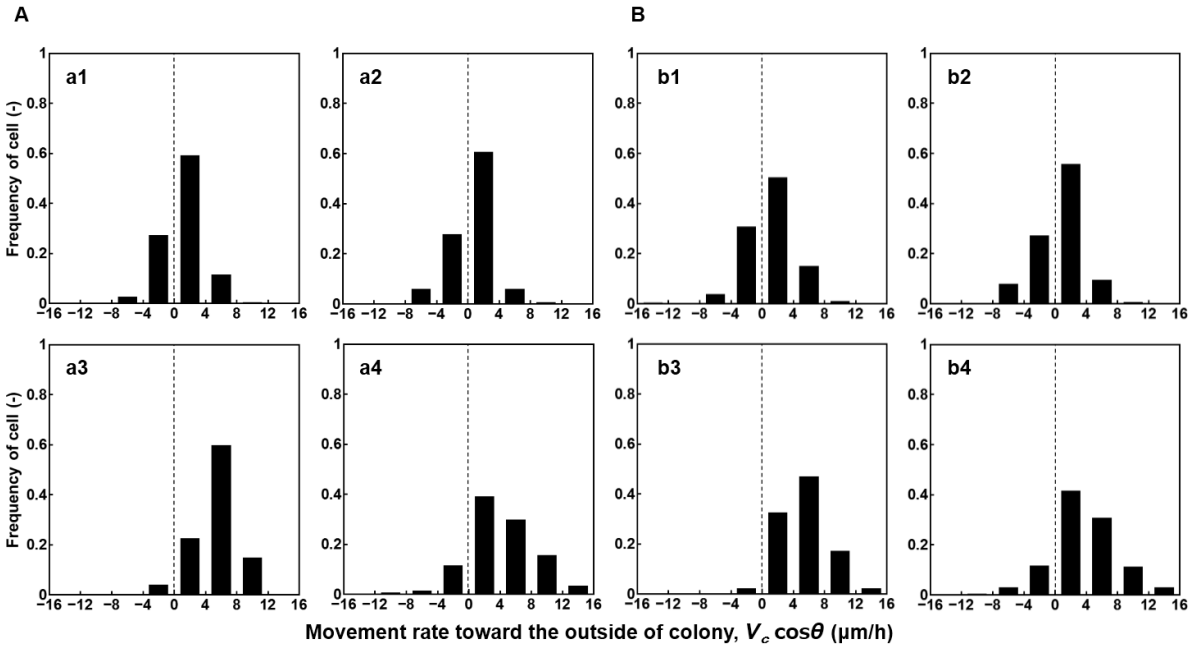

Figure 2.6 Frequencies of cell against movement rate toward the outside of colony $V_c \cos\theta$ at 48-54 h at the central region (a1, a2, b1, b2) and peripheral region (a3, a4, b3, b4) of the hiPSC colonies when cultured *in silico* (a1, b1, a3, b3) and *in vitro* (a2, b2, a4, b4) on SNL (A) and MEF (B) feeder cells.

2.3.4 Elucidation of cell movement behavior in colonies

The spatial and temporal dependence of cell movement rate were analyzed to understand the heterogeneity of cell movement rates in hiPSC colony. The average movement rates $\overline{V_R}$ of all cells from single colonies cultured on MEF feeder cells were calculated at every 100 μm from the center of the colony at t = 50 h, 90 h, and 128 h where the colony radiuses equaled 300 μm, 500 μm, and 700 μm, respectively (**Fig. 2.7**). Two distinct parts of cells including quiescent cells at the central region of the colony and proliferating cells at the peripheral region of the colony were observed (**Fig. 2.7a1,b1,c1**). As time passed, a contact inhibition region expanded but the width of proliferating at the peripheral region of colony remained constant. At t = 50 h, $\overline{V_R}$ increased as the distance from the center of the colony R increased (**Fig. 2.7a2**). At t = 90 h and 128 h, $\overline{V_R}$ were homogeneous in the contact inhibition region but heterogeneous in the proliferating ring at the edge of the colony. In addition, $\overline{V_R}$ in the contact inhibition region did not change as colony grew. In contrast, in proliferating rings, it gradually increased inside out to the edge of the colony. This result indicated the temporal independence and spatial dependence of the average cell movement rate in a colony of hiPSCs.

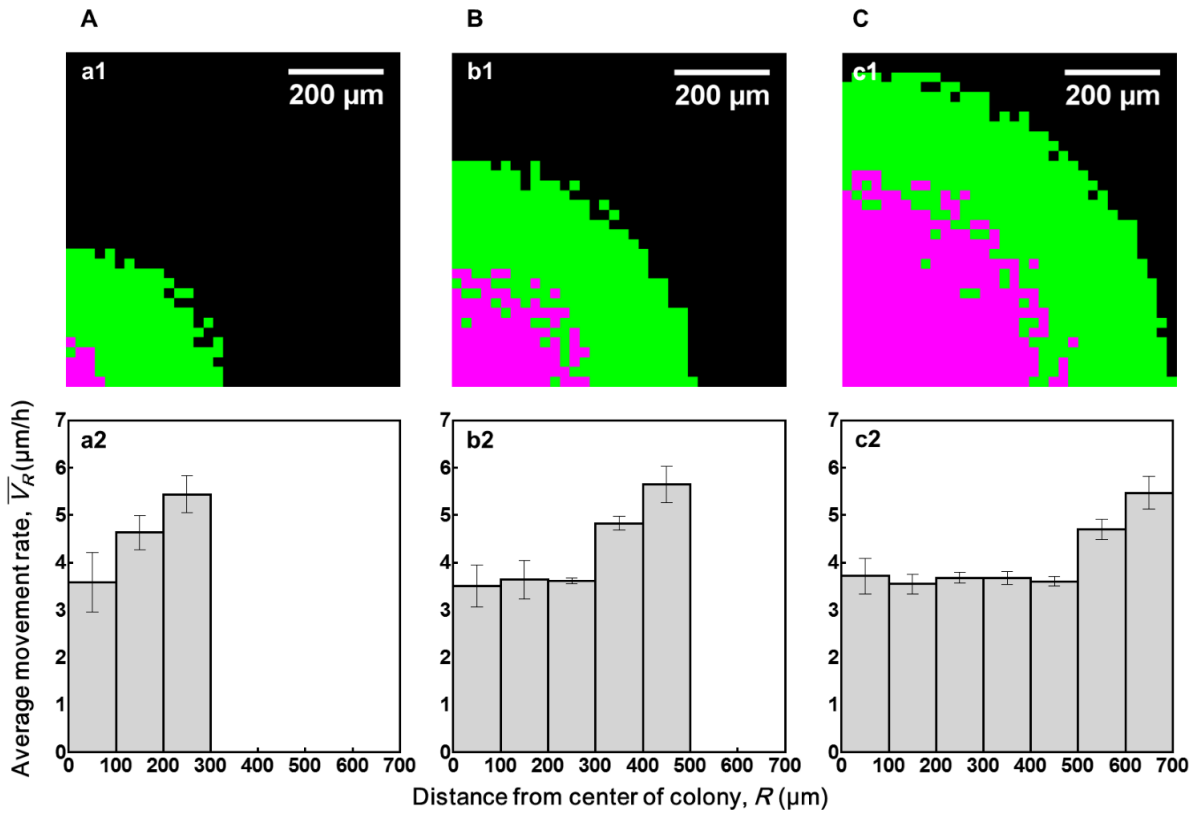

Figure 2.7 *In silico* results at 50 h (A), 90 h (B), and 128 h (C): state of cells in a colony (a1, b1, c1) (pink: quiescent state, green: proliferating state); average movement rate against the distance from the center of the colony (a2, b2, c2)

The difference in $\overline{V_R}$ between the contact inhibition region and proliferating region in **Fig. 2.7** implied that cell division might be the factor that leads to the spatial heterogeneity of cell movement in colonies. Therefore, cell division was stopped by setting the value of $\overline{t_g}$ to infinity and cell migration was stopped by setting the value of $V_{m,free}$ to zero to clarify that speculation. **Fig. 2.8** showed the heat map of the cell movement rate V_c and $\overline{V_R}$ at t = 128 h when the colony radius reached 700 μm. In the contact inhibition region, $\overline{V_R}$ was always homogeneous and decreased to zero only when cell migration was stopped (**Fig. 2.8C**). In the proliferating ring of the colony, $\overline{V_R}$ decreased but was still heterogeneous when cell migration was stopped (**Fig. 2.8C**) and became homogeneous only when cell division was stopped (**Fig. 2.8B**). This result

suggested that cell division was a key factor that led to the spatial heterogeneity of cell movement in colonies.

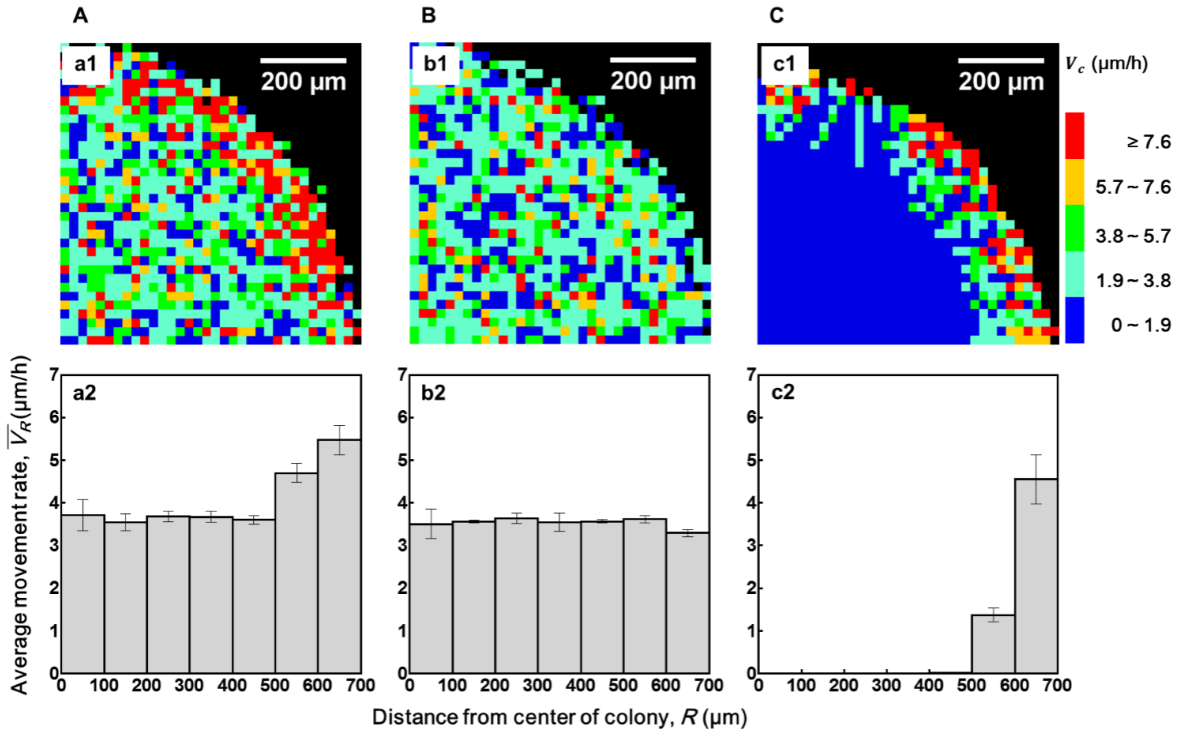

Figure 2.8 *In silico* results when hiPSC colonies were cultured on MEF feeder cells under control conditions (A), when cell division was stopped (B), and when cell migration was stopped (C): heat map for movement rate of individual cells in one colony at 128 h (a1, b1, c1); average movement rate against the distance from the center of the colony (a2, b2, c2). Blue cell: $0 \leq V_c < 1.9$, cyan cell: $1.9 \leq V_c < 3.8$, green cell: $3.8 \leq V_c < 5.7$, orange cell: $5.7 \leq V_c < 7.6$, red cell: $7.6 \leq V_c$.

To understand the effect from cell division, positions of some cells at the central and peripheral regions of colonies were tracked. The results showed that cells at the central region of colonies (yellow cells) fluctuated around the center of the colony while cells at the peripheral region of the colony (red cells) migrated toward the edge of the colony (**Fig. 2.9A**). The frequency of cell pushing every 24 h was also calculated to explain the effect of cell pushing on cell movement. At the central region of the colony, no cell pushing was found during *in silico* culture (**Fig. 2.9B**). In contrast, cells at the peripheral region of the colony were pushed

by the division of inner cells at the frequency around 0.27 times/h (**Fig. 2.9C**). At the same time, the average cell movement rate at the peripheral region of the colony was higher than that at the central region of the colony. This result indicated a proportional relationship between the frequency of cell pushing and the cell movement rate in colonies of hiPSCs.

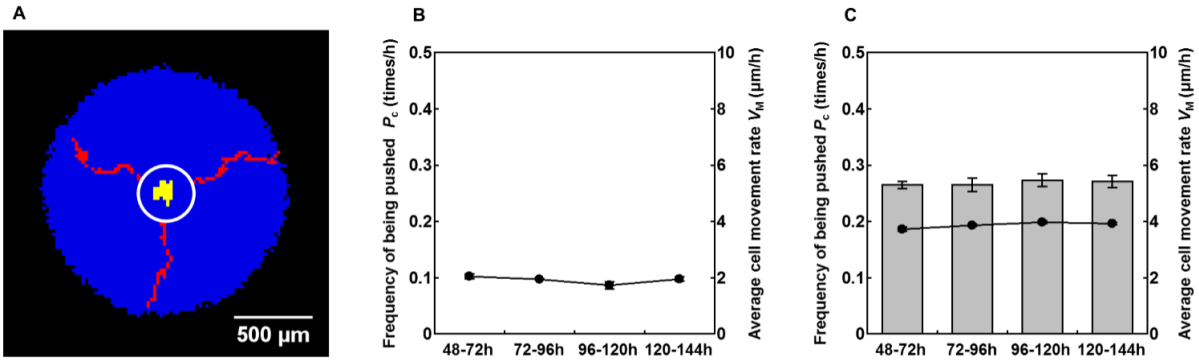

Figure 2.9 *In silico* movement trajectory of three representative cells at the central region and at the peripheral region of the colony from t = 24 h to t = 144 h (A); *in silico* frequencies of cell pushing (grey column) and cell movement rate (black line) at the central region (B) and peripheral region (C) of the colony. Yellow cells: cells at the central region of colony at t = 24 h; red cells: cells at the peripheral region of colony at t = 24 h; blue cells: non-tracked cells at t = 144 h; white ring: edge of colony at t = 24 h

2.4 Discussion

Pursuing the idea of controlling hiPSC fate through migration-dependent regulation of the balance between cell-cell and cell-substrate connections (Kim and Kino-oka 2015), I have described it in a kinetic model for the first time. The maximum energy E_{max}, which is specific for each cell line, is used by cells to make connections and migrations. Connection energy and energy for migration sound similar to physical potential energy and kinetic energy. Even though they could not be measured directly from *in vitro* experiments in this work, what important is the balance between them. Furthermore, current researches showed quantitative measurement of cell-cell connection and cell-substrate connection strength by using atomic force microscope

(Moreno-Cencerrado et al. 2016) that makes this kinetic model accessible in future. Fitting to experimental results showed that hiPSCs cultured on SNL feeder cells had different state of balance between cell-cell connection energy and cell-substrate connection energy compared to hiPSCs cultured on MEF feeder cells. I believe that different feeder cells provided distinct topology surrounding hiPSCs that led to different cell-substrate connection energies and then indirectly affected cell-cell connection. Moreno-Cencerrado et al. (2016) also reported that the strength of the cell-cell connection was highly influenced by the strength of the cell-substrate connection. The number of cell layers for occurrence of contact inhibition N_c was also estimated by fitting to *in vitro* data. The result showed a lesser degree of contact inhibition in hiPSC cultures than in non-stem cell cultures as reported previously (Kino-oka et al. 2000, Kagawa and Kino-oka 2016) where N_c equaled 1.

With the well-validated model, simulations were executed to understand the reason for the spatial heterogeneity of average cell movement rate in colonies. I first found the difference in movement behavior between the contact inhibition region and the proliferating region that implied the role of cell division in cell movement rates in a colony. By stopping cell migration or cell division, the result showed that both cell migration and cell division affected cell movement rates in a colony. However, only cell division led to a higher cell movement rate at the peripheral region of the colony than at the central region of the colony. The cell pushing mentioned in this chapter came from the division rule where the mother cells push neighboring cells to make space for their daughter cells when there is no vacant space around the cell that was also used in some models of cancer cells (Stephanou et al. 2017, Forster et al. 2017).

In this chapter, there is a need to distinguish between two terms: cell migration and cell movement. Cell migration is the ability of a cell to actively change to a new position that is described cell behavior in this kinetic model. Meanwhile, cell movement is the overall cell displacement that may result from cell migration or by being pushed by cell division. In the

contact inhibition region, cell movement rate was only affected by cell migration. In contrast, at the peripheral region of the colony, cell movement rate was affected by both cell migration and cell division.

Using cellular automata approach, this kinetic model has a disadvantage in simulating continuous processes such as cell migration. *In silico* cells do not continuously change their positions, but immediately change of their position at a time point then wait in the new position for a period of time. In addition, it is impossible to realize an increase in cell size during growth, mechanical constraint of cells in a population, or the multi-directionality of cell migration. On the other hand, the strength of CA is lower computational cost than off-lattice models. More importantly, CA helps to realize the heterogeneity of cell population that is impossible when using a continuous model.

2.5 Summary

I have developed a kinetic model to clarify the origin of the spatial heterogeneity in cell migration which was difficult to understand by *in vitro* studies alone. With cellular automaton approach, I described fundamental cell behaviors including cell division, contact inhibition, cell migration, cell–cell connections, and cell–substrate connections. All parameter values were estimated from *in vitro* data and the appropriateness of the kinetic model was indicated by good agreement between *in silico* output and *in vitro* data. Executed *in silico* experiments, I found that the cell division was the main cause of the observed spatial heterogeneity. This result indicated that there is a need to separate components of *in vitro* cell migration before considering the actual trigger for the deviation from the undifferentiated state.

Chapter 3 Modelling the deviation from the undifferentiated state of hiPSCs

3.1 Introduction

Normally, undifferentiated hiPSCs are expanded as monolayer colonies in culture with feeder cells. In 2014, the deviation from the undifferentiated state of hiPSCs was reported by Kim et al., in culture with two types of feeder cells. In culture with SNL feeder cells, the deviation from the undifferentiated state was observed at the central region of colonies and occurred with higher probability at the bigger colonies. In culture with MEF feeder cells, however, the deviation from the undifferentiated state was observed at the peripheral region of colonies and occurred equally at different colony sizes. The deviated cells not only lost pluripotent characteristics but also were negative for markers of three germ layer (Kim et al. 2017).

To understand the fundamental mechanisms that trigger deviation from the undifferentiated state of hiPSCs, Shuzui et al., (2019a) analyzed cell migration rate at the central and peripheral region of colonies cultured with above feeder cells. The deviated colonies were exposed to a Rac1 activator (HMG1) or inhibitor (NSC23766) in order to activate or inhibit cell migration, respectively. This result was the motivation of their study and indicated that changes in cell migration could trigger deviation from the undifferentiated state of hiPSCs. They then obtained colonies with additional occurrence of deviation at the peripheral and central region in incubation with Rac1 activator and inhibitor, respectively. When compared the distribution of cell migration rates, they found more slow or fast migrating cells in central and peripheral regions, respectively, in deviated colonies, compared to colonies that maintained their pluripotency (**Fig. 3.1**). Besides, the cytoskeletal rearrangement and accumulation of nuclear laminA/C through imbalance between cell-cell and cell-substrate adhesions was found at the central and peripheral regions of colonies. Consequently, heterochromatin might be formed during nuclear lamina assembly and led to modulation of gene transcription (Underwood et al. 2017). After all, Shuzui et al. came up with the hypothesis

that anomalous cell migration acts as a key trigger for deviation from the undifferentiated state of hiPSC colonies.

However, sequential cell migration before deviation is difficult to observe *in vitro*, suggesting the need for a kinetic model to understand this phenomenon. The study by Shuzui et al. suggested the existence of anomalous cell migration, but was unable to exactly define that anomaly. Also, from result of chapter 2, we have known that components of *in vitro* cell migration contributed differently on overall cell migration that raised the question about the actual trigger for the deviation from the undifferentiated state. In this chapter, I analyzed not only apparent movement, which had similar meaning to *in vitro* cell migration, but also constituent movements, including movement caused by active migration, movement caused by passive migration, and movement caused by cell division, to assess the potential triggers. In addition to the developed modules explained in chapter 2, I further constructed a deviation module that describes the generation of deviated cells. Even though there have been many factors could be related to the deviation of hiPSCs such as cell migration, cell-cell and cell-substrate interactions, cell morphology, and nuclear lamina (Kim et al. 2014, Shuzui et al. 2019), the model used cell migration as a key factor. This consideration adopted previous *in vitro* hypothesizes about mechanisms for occurrence of hiPSC deviation developed by Kim et al. (2014) and Shuzui et al. (2019). In this chapter, hiPSC deviation was explained by two factors: mechanical stimulus, represented by cell movement, and duration of mechanical stimulus. The simulation was then executed to see if the developed model could recapitulate several properties of hiPSC deviation.

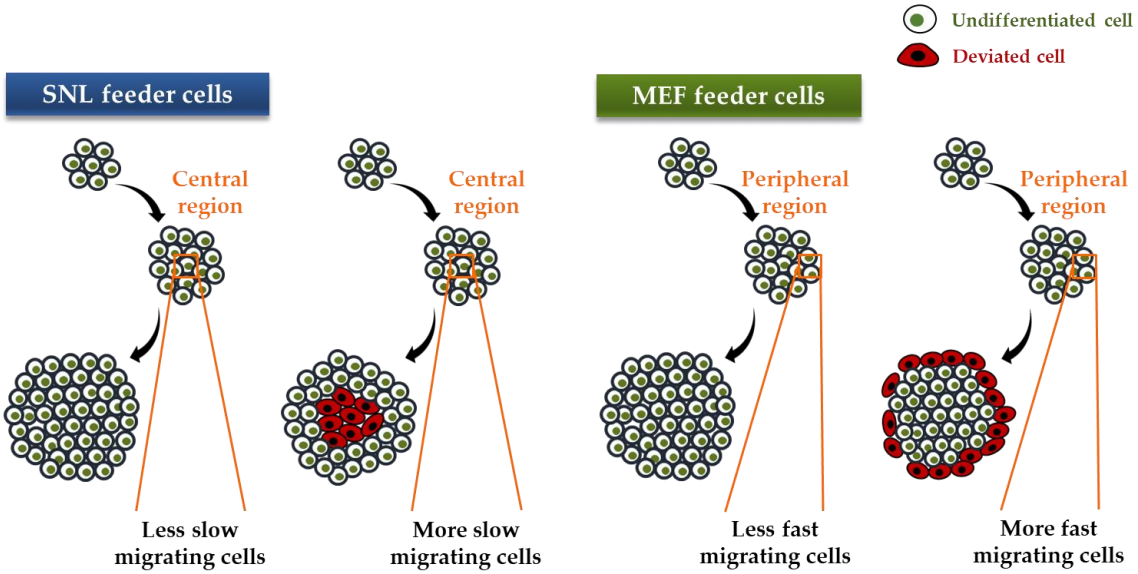

Figure 3.1 Schematic drawing of *in vitro* finding that there are more slow migrating cells at the central region and fast migrating cells at the peripheral region of undifferentiated colonies than of deviated colonies (Shuzui et al. 2019a).

3.2 Materials and Methods

3.2.1 *In vitro* culture of hiPSCs

In vitro culture of hiPSCs was similar to what mentioned in chapter 2. To block E-cadherin interactions, hiPSCs were cultured with SNL feeder cells for 48 h, and then 50 nM botulinum hemagglutinin (HA) complex was added. More details of culture methods are described in previous papers (Shuzui et al. 2019b).

3.2.2 *In silico* culture of hiPSCs

In silico culture of hiPSCs was performed using cellular automata approach in which each cell was represented by one hexagonal prism (**Fig. 3.2**). Each cell had maximum six neighboring prisms, and seven underlying substrate prisms. Custom C# code in a Visual Studio environment (Microsoft, Redmond, Washington, USA) was created to simulate on a commercially available workstation (Precision T7920 workstation, Dell Inc., Round Rock, Texas, USA). Space of

culture vessel was sized to simulate a standard 24-well plate (culture area in each vessel: 1.9 cm^2; Corning Costar, Cambridge, MA, USA). Initial colony number and colony size in one culture vessel were estimated from *in vitro* data. Computational calculations were performed at every time step (t_{step} = 0.1 h).

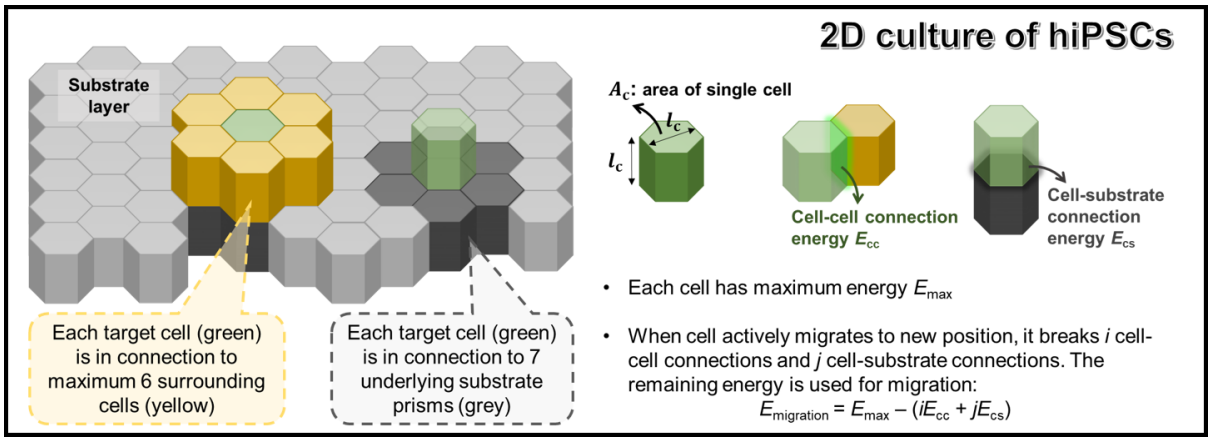

Figure 3.2 Schematic of our model illustrating the definitions of cell connections and cell migration in case each cell is presented by a hexagonal prism.

In this chapter, the rules for cell migration are similar to those mentioned in a previous chapter except that a cell can migrate in one of six distinct directions (N_d = 6) denoted by the variable dir. The apothem length of the base of a hexagonal prism l_c, mean generation time $\bar{t_g}$, the number of cell layers for the occurrence of contact inhibition N_c, free migration rate $V_{m,free}$, ratio of energy for a cell-cell connection ε_{cc}, and ratio of energy for a cell-substrate connection ε_{cs} were estimated again using methods described in chapter 2 (**Table 2, Fig. S1–2**). Additionally, the rule for cell death was also considered because no single cell was observed *in vitro*. The rule states that an undifferentiated hiPSC dies if it does not connect with any neighboring cells.

Table 2 *in silico* parameters for undifferentiated cells cultured on SNL and MEF feeder cells

Variable	Symbol	Unit	Value
Apothem length of the base of a hexagonal prism	l_c	μm	19.5 (SNL), 22.2 (MEF)
Mean generation time	$\bar{t_g}$	h	15.8 (SNL), 21.5 (MEF)
The number of cell layers for the occurrence of contact inhibition	N_c	cell layer	8 (SNL), 11 (MEF)
Free migration rate	$V_{m,free}$	μm/h	8.0
Ratio of energy for cell-cell connection	ε_{cc}	-	0.07 (SNL), 0.05 (MEF)
Ratio of energy for cell-substrate connection	ε_{cs}	-	0.21 (SNL), 0.16 (MEF)

3.2.3 Calculation of different types of hiPSC movement rate within a colony

In silico cell movement rates caused by active migration (V_{act}), passive migration (V_{pas}), cell division (V_{div}), and the apparent movement rate (V_{app}) were calculated as follows (**Fig. 3.3**): when there is a cell displacement due to active migration at time t, V_{act} is calculated as $\frac{l_{act}}{t_{act}}$, where l_{act} is the most recent displacement due to active cell migration (at time $t - t_{act}$) and t_{act} is the time interval between consecutive active migrations. If at time t, there is a cell displacement due to passive migration, V_{pas} is calculated as $\frac{l_{pas}}{t_{pas}}$, where l_{pas} is the most recent displacement due to passive cell migration (at time $t - t_{pas}$) and t_{pas} is the time interval between consecutive passive migrations. V_{div} is calculated as $\frac{l_{div}}{t_{div}}$, where l_{div} is the most recent cell division displacement (at time $t - t_{div}$) and t_{div} is the time interval between two divisions if there is a cell displacement due to cell division at time t. Lastly, V_{app} is calculated as $\frac{l_{app}}{t_{app}}$,

where l_{app} is the most recent displacement (at time $t - t_{app}$) and t_{app} is the time interval between those events.

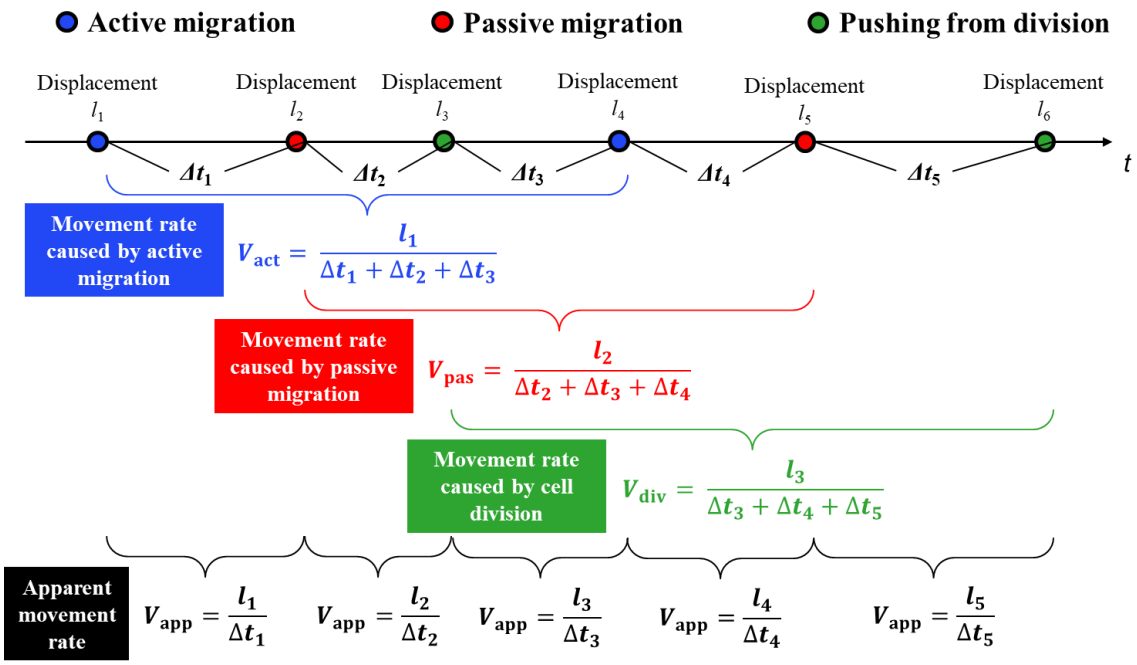

Figure 3.3 Schematic drawing of method for calculating different types of cell movement rate

3.2.4 Analysis of the trigger for hiPSC deviation within colonies

Culture of fifty *in silico* colonies were performed on MEF feeder cells for 120 h with an initial colony size of 300 cells/colony. The average V_{act}, V_{pas}, V_{div}, and V_{app} at each position of those colonies were calculated and presented as heat maps. Based on *in vitro* finding (Kim et al. 2014), types of movement that could possibly initiate deviation at the central and peripheral regions of colonies were decided by different criteria. A movement type that could trigger deviation at the central region of a colony must meet two criteria: (i) the area of the region with the lowest cell movement rate at the central region of a colony must increase as time passes, (ii) cell movement rate at the central region must differ from zero. In contrast, the one that may trigger deviation at the peripheral regions must show a constant higher movement rate over

time. Besides, V_{act} is believed to have a stronger influence on cell fate than V_{pas} because it relates to energy consumption.

3.2.5 Fitting method

Least-squares fitting was used to find the best fit values for the critical times for occurrence of deviation due to low V_{app} or high V_{act} ($t_{\mathrm{de,app}}$, $t_{\mathrm{de,act}}$).

3.3 Results

3.3.1 Kinetic modeling of the module that describes the generation of deviated cells via anomaly index

50 *in silico* colonies were cultured on MEF feeder cells for 120 h with the initial colony size of 300 cells/colony, and the heat maps of movement rate caused by active migration V_{act}, movement rate caused by passive migration V_{pas}, movement rate caused by cell division V_{div}, and apparent movement rate V_{app} of these colonies were overlapped. From **Fig. 3.4**, a ring of cells at the edge of colony showing different movement rate was observed in case of V_{act} and V_{pas} (**Fig. 3.4A,B**). On the other hand, both V_{div} and V_{app} showed the gradual increase from the central region of colony to the peripheral region of colony, and the region of the lowest movement rate at the central region of colony expanded as colony grew (**Fig. 3.4C,D**). However, the lowest passive movement rate at the central region was zero because of the contact inhibition where no cell division occurred.

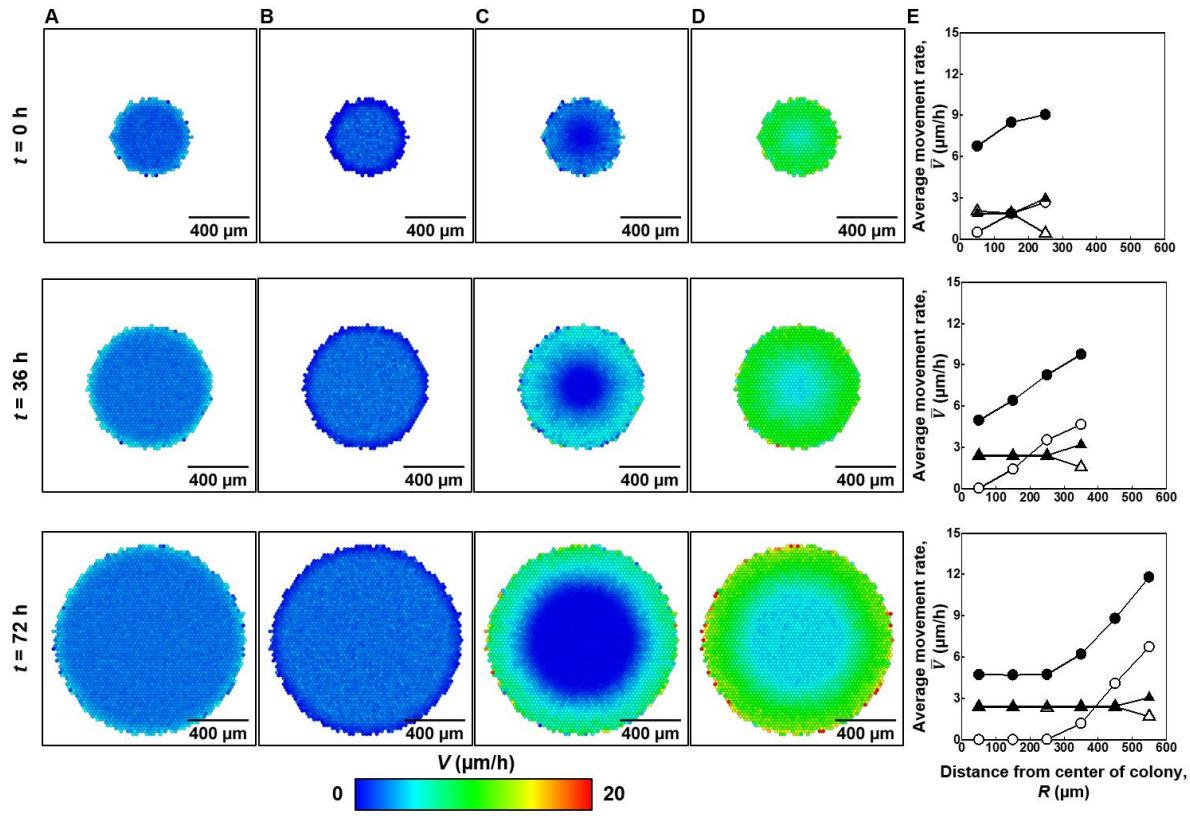

Figure 3.4 Heat maps of cell movement rate caused by active migration (V_{act}) (A), cell movement rate caused by passive migration (V_{pas}) (B), movement rate caused by cell division (V_{div}) (C), and apparent cell movement rate (V_{app}) (D) at 0, 36, and 72 h. The graphs show average V_{act} (closed triangles), average V_{pas} (open triangles), average V_{div} (open circles), and average V_{app} (closed circles) plotted against distance from the center of a colony (E).

Based on this *in silico* analyses, it was suggested that apparent movement rate (V_{app}) and movement rate caused by active migration (V_{act}) were related to the deviation at the central and peripheral region of colony, respectively. Therefore, it was hypothesized that the deviation is triggered by a continuous low apparent movement rate (V_{app}) or a continuous high movement rate caused by active migration (V_{act}). The rules for occurrence of deviation are explained as follows (**Fig. 3.5**).

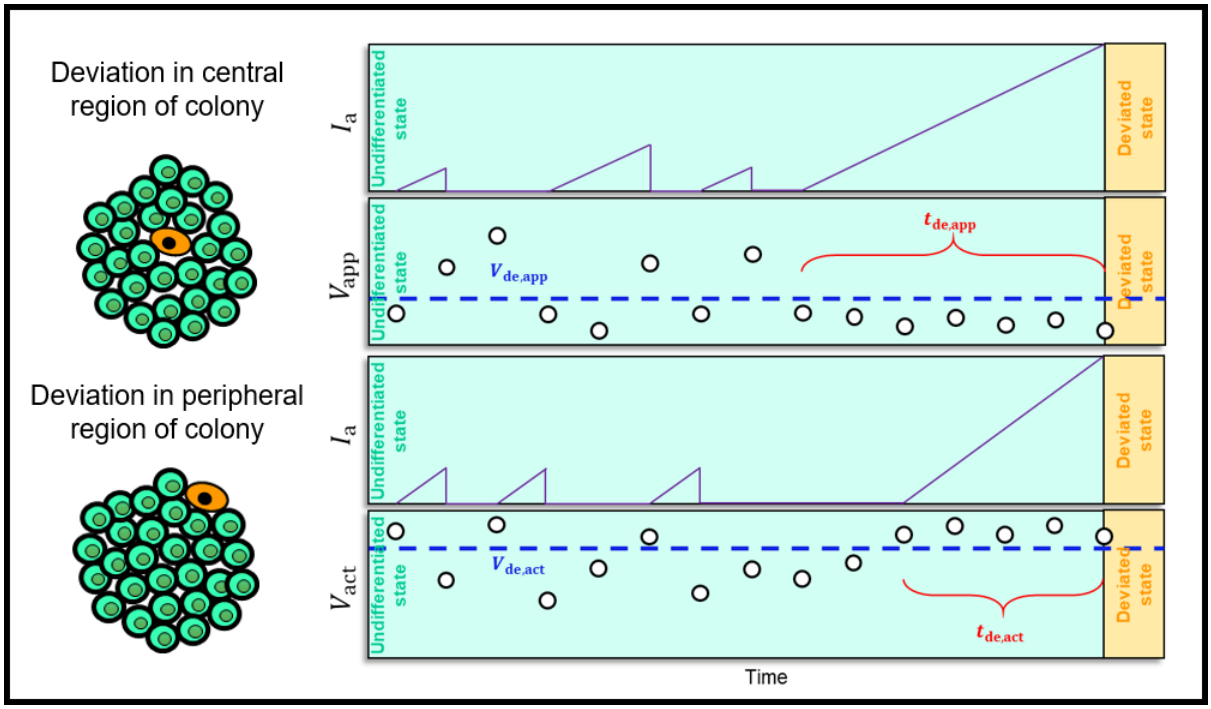

Figure 3.5 Schematic of our model that describes the rule for initiation of deviation. Green cells: undifferentiated cells; orange cells: deviated cells.

Each cell has a cumulative duration of a low V_{app}, $T_{\mathrm{ac,app}}(t)$, at each time t that is calculated every time step:

$$T_{\mathrm{ac,app}}(t) = \begin{cases} T_{\mathrm{ac,app}}(t - t_{\mathrm{step}}), & \text{there is no cell displacement} \\ T_{\mathrm{ac,app}}(t - t_{\mathrm{step}}) + t_{\mathrm{app}}, & V_{\mathrm{app}} < V_{\mathrm{de,app}} \\ 0, & V_{\mathrm{app}} \geq V_{\mathrm{de,app}} \end{cases} \tag{11}$$

where $V_{\mathrm{de,app}}$ is the lower threshold of V_{app}. When $T_{\mathrm{ac,app}}$ exceeds the threshold $t_{\mathrm{de,app}}$, cell start to deviate from the undifferentiated state.

Each cell has a cumulative duration of a high V_{act}, $T_{\mathrm{ac,act}}(t)$, at each time t that is recalculated every time step:

$$T_{\mathrm{ac,act}}(t) = \begin{cases} T_{\mathrm{ac,act}}(t - t_{\mathrm{step}}), & \text{there is no cell displacement} \\ T_{\mathrm{ac,act}}(t - t_{\mathrm{step}}) + t_{\mathrm{act}}, & V_{\mathrm{act}} > V_{\mathrm{de,act}} \\ 0, & V_{\mathrm{act}} \leq V_{\mathrm{de,act}} \end{cases} \tag{12}$$

where $V_{\mathrm{de,act}}$ is the upper threshold of V_{act}. When $T_{\mathrm{ac,act}}$ exceeds the threshold $t_{\mathrm{de,act}}$, cell start to deviate from the undifferentiated state.

$T_{\mathrm{ac,app}}$ and $T_{\mathrm{ac,act}}$ are parameters for real-time detection of the cumulative duration of a low V_{app} or a high V_{act}. These two parameters have discrete values because they change only when cell displacement occurs. Thus, $T_{\mathrm{re,ac,app}}$ and $T_{\mathrm{re,ac,act}}$, the retrospective cumulative duration of a low V_{app} or a high V_{act}, were also used to understand the continuous cumulative duration. Then, the anomaly index of each cell, I_{a}, is estimated as $T_{\mathrm{re,ac,app}}/t_{\mathrm{de,app}}$ or $T_{\mathrm{re,ac,act}}/t_{\mathrm{de,act}}$ in culture on SNL and MEF feeder cells, respectively.

3.3.2 Estimation of parameter values

Parameters used in deviation rules were estimated as follows: $V_{\mathrm{de,app}}$ was estimated as the 25th percentile value of the *in vitro* cell migration rate at the central region of undifferentiated colonies cultured on SNL feeder cells and equaled 2.1 μm/h (Shuzui et al. 2019a). $V_{\mathrm{de,act}}$ was estimated as the 75th percentile value of *in silico* V_{act} (4.9 μm/h) because the corresponding *in vitro* data was not available. $t_{\mathrm{de,app}}$ and $t_{\mathrm{de,act}}$ were estimated by fitting to the *in vitro* average frequency of deviation in one culture vessel. About 200 *in silico* colonies were cultured following *in vitro* colony size distribution (**Fig. S3**). The values of $t_{\mathrm{de,app}}$ and $t_{\mathrm{de,act}}$ were changed from 1 h to 96 h and to find the value giving the most similar deviation frequency to *in vitro* data. As the result, $t_{\mathrm{de,app}}$ was estimated as 48 h where deviation frequency at the central region of a colony was 15.4 ± 2.8% when cultured on SNL feeder cells (**Fig. 3.6A**) but negligible when cultured on MEF feeder cells. $t_{\mathrm{de,act}}$ was estimated as 38 h where the deviation frequency at the peripheral region of a colony was 14.5 ± 4.3% when cultured on MEF feeder cells (**Fig. 3.6B**), but 0% when cultured on SNL feeder cells.

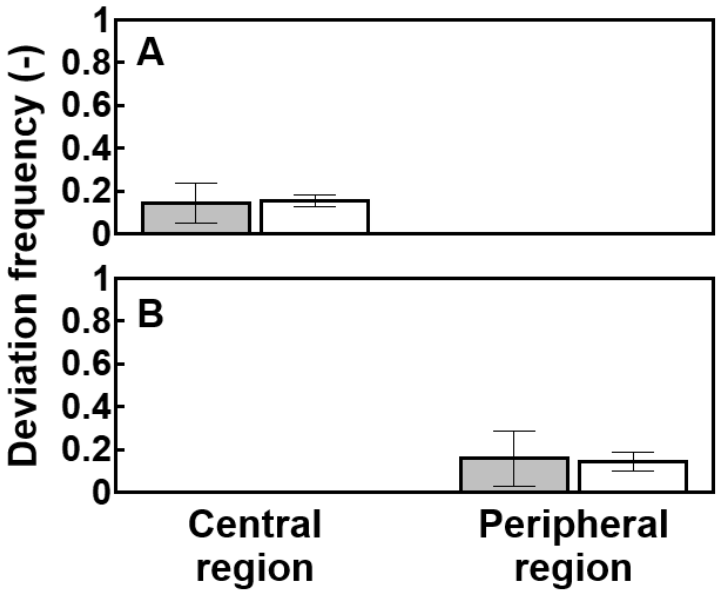

Figure 3.6 Estimation of $t_{\mathrm{de,act}}$ and $t_{\mathrm{de,app}}$ via fitting deviation frequencies in the central and peripheral regions of hiPSC colonies cultured on SNL (A) and MEF (B) feeder cells. Grey bars: *in vitro* results (14); white bars: best fit *in silico* results obtained via least-squares fitting. Standard deviations were calculated from three culture batches (about 200 single colonies/batch).

3.3.3 Model validation

Firstly, the positions of deviated cells in *in silico* colonies were compared to that *in vitro* to validate the model. The blue cells, which had deviated due to continuous low V_{app}, were found at the central region of the colonies cultured on SNL feeder cells (**Fig. 3.7A**). The green cells, which had deviated due to continuous high V_{act}, were found at the peripheral region of colonies cultured on MEF feeder cells (**Fig. 3.7C**). One hundred colonies with deviated cells from both culture conditions were analyzed to understand positions within colonies where deviation was most likely to occur. Deviated cells were mostly at the central region of colonies cultured on SNL feeder cells and at the peripheral region of colonies cultured on MEF feeder cells (**Fig. 3.7B, D**). These results were in agreement with *in vitro* locations of deviated cells.

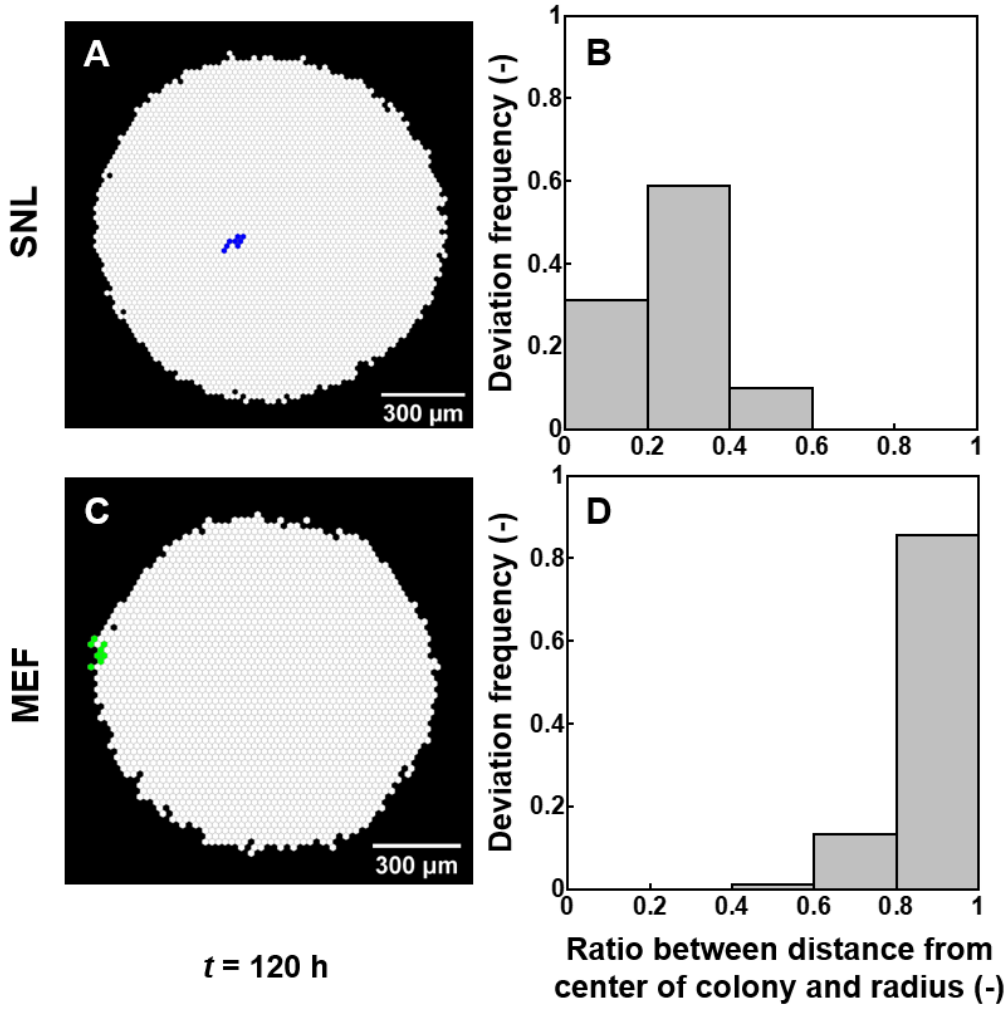

Figure 3.7 *in silico* morphology of colonies with deviated cells cultured on SNL (A) and MEF (C) feeder cells at t = 120 h. The graph shows the deviation frequency at different positions in colonies cultured on SNL (B) and MEF (D) feeder cells. White cells: undifferentiated cells; blue cells: cells that had deviated due to low V_{app}; green cells: cells that had deviated due to high V_{act}.

Secondly, *in vitro* and *in silico* time profiles for colonies with and without deviated cells were compared. With about 200 *in silico* colonies were cultured on SNL or MEF feeder cells, the experiment was performed three times. Twenty-six and 27 representative undifferentiated colonies and deviated colonies were selected in cultures on SNL and MEF feeder cells, respectively. Average size of undifferentiated colonies was calculated every 6 hours since the beginning of culture, size of each deviated colonies was determined at times of deviation. In

deviated colonies cultured on SNL feeder cells, the ratio between colonies larger than the average undifferentiated colony and smaller than the average undifferentiated colony was 16:1 (**Fig. 3.8A**). In culture on MEF feeder cells, this ratio was 1:3 (**Fig. 3.8B**). In *in vitro* culture on SNL and MEF feeder cells, these ratios were 8:1 and 5:8, respectively. Both ratios 8:1 (*in vitro*) and 16:1 (*in silico*) indicated the colony-size dependent manner of deviated colonies in culture on SNL feeder cells. On the other hand, both ratios 5:8 (*in vitro*) and 1:3 (*in silico*) implied the colony size-independent manner of deviated colonies in culture on MEF feeder cells. These *in silico* results showed similar trend to *in vitro* results.

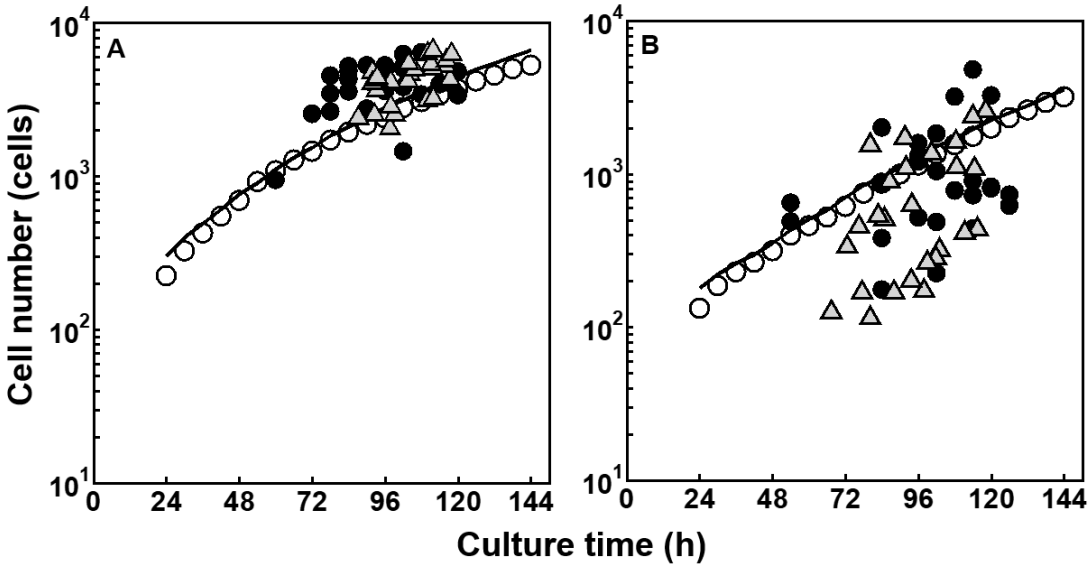

Figure 3.8 Time profiles of hiPSC colonies with and without deviated cells in cultures on SNL (A) and MEF (B) feeder cells for t = 144 h. Open circles represent *in vitro* colonies without deviated cells (14). Closed circles represent *in vitro* colonies with deviated cells (14). Lines represent *in silico* colonies without deviated cells. Triangles represent *in silico* colonies with deviated cells. Closed circles and triangles indicate timing of appearance of deviated cells in hiPSC colonies.

Finally, *in silico* strength of cell-cell connections was altered at the beginning of culture on SNL feeder cells. Previously, Shuzui et al. (2019b) showed that the average *in vitro* cell migration rate at the central region of a colony increased by 0.5 μm/h when cells were cultured

in medium supplemented with 50 nM HA. In that culture condition, no deviation was observed. The ratio of cell-cell connection energy (ε_{cc}) was decreased by $\Delta\varepsilon_{cc}$ (-) = [0.01, 0.06]. About 200 colonies were cultured in each condition and the experiments were performed three times. The deviation frequency at the central regions of colonies was 0.15 ± 0.03 under normal culture conditions ($\Delta\varepsilon_{cc}$ = 0) (**Fig. 3.9A**). This frequency drastically decreased to 0.08 ± 0.01 when ε_{cc} was decreased by 0.01. When ε_{cc} was decreased by 0.02, 0.03, or 0.04, this frequency of decreased further to approximately 0.01. Finally, when ε_{cc} was very small ($\Delta\varepsilon_{cc}$ = 0.05, 0.06), no deviation in the central regions of colonies was detected in culture. With $\Delta\varepsilon_{cc}$ = 0.05, I obtained 0.5 μm/h higher average V_{app} at the central regions of colonies no deviation that was similar to *in vitro* results. *In silico* cultures under normal conditions on SNL feeder cells ($\varepsilon_{cc} = 0.07$) and with addition of HA ($\varepsilon_{cc} = 0.02$) were performed in 1000 vessels. Only 20 vessels contained deviated colonies (2%) under conditions simulating HA addition, while that number was 983 vessels under normal conditions (98.3%) (**Fig. 3.9B**).

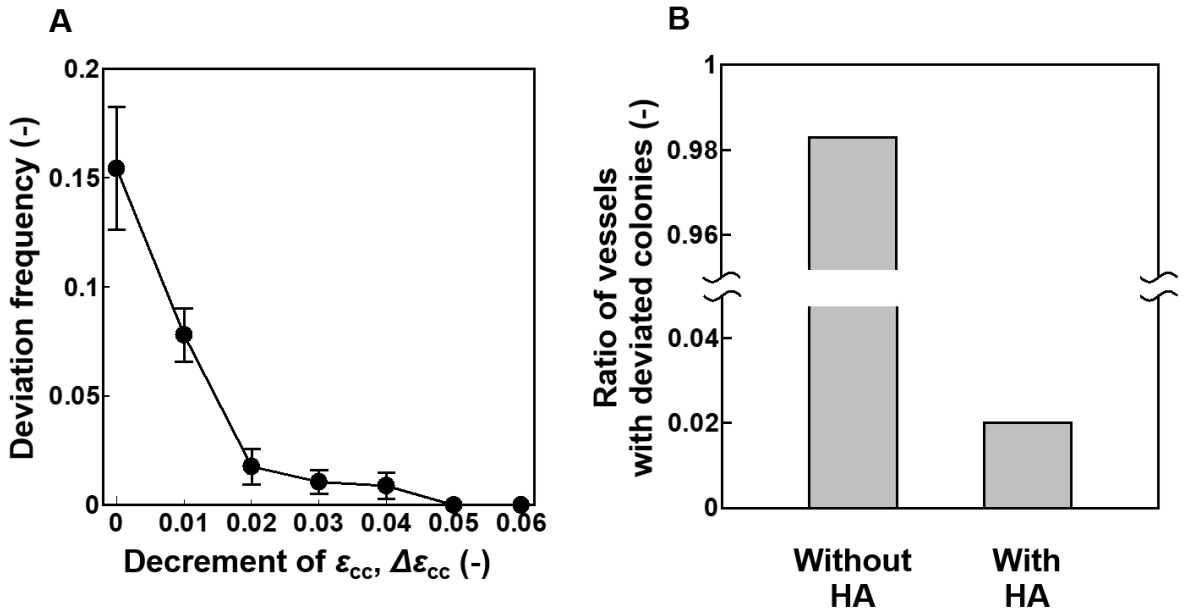

Figure 3.9 A. *in silico* deviation frequency plotted against the decrement of the ratio of cell-cell connection energy ($\Delta\varepsilon_{cc}$.). Standard deviations were calculated from three culture batches

(about 200 single colonies/batch). B. *in silico* deviation frequency in cultures with or without HA addition calculated from 1000 culture vessels.

3.3.4 Elucidation of deviation using anomaly index

With the well-validated model, further analyses were performed to understand about the trigger of deviation from the undifferentiated of hiPSCs using anomaly index. In the representative colony cultured on SNL feeder cells, one cell at the central region of colony deviated after its I_{a} reached 1 (**Fig. 3.10B**). One cell at the peripheral region of the representative colony cultured on MEF feeder cells deviated when its I_{a} hit 1 (**Fig. 3.10E**). Later, retrospective tracking of 15 deviated cells and their neighbors was performed to understand their relationship to their microenvironment. For cells cultured on SNL feeder cells, the tracking time $t' = t_{\mathrm{de,app}}$ when I_{a} of the deviated cell was equal to 1. For cells cultured on MEF feeder cells, the tracking time $t' = t_{\mathrm{de,act}}$ when I_{a} of the deviated cell equaled 1. The result showed that when I_{a} of deviated cells gradually increased since $t' = 0$ h, the average I_{a} of their neighbors also increased since $t' = -24$ h and become saturated later in cultures on SNL feeder cells (**Fig. 3.10C**). In cultures on MEF feeder cells, even though I_{a} of deviated cells gradually increased since $t' = 0$ h, the average I_{a} of their neighbors fluctuated and did not show a clear trend during the tracking period (**Fig. 3.10F**).

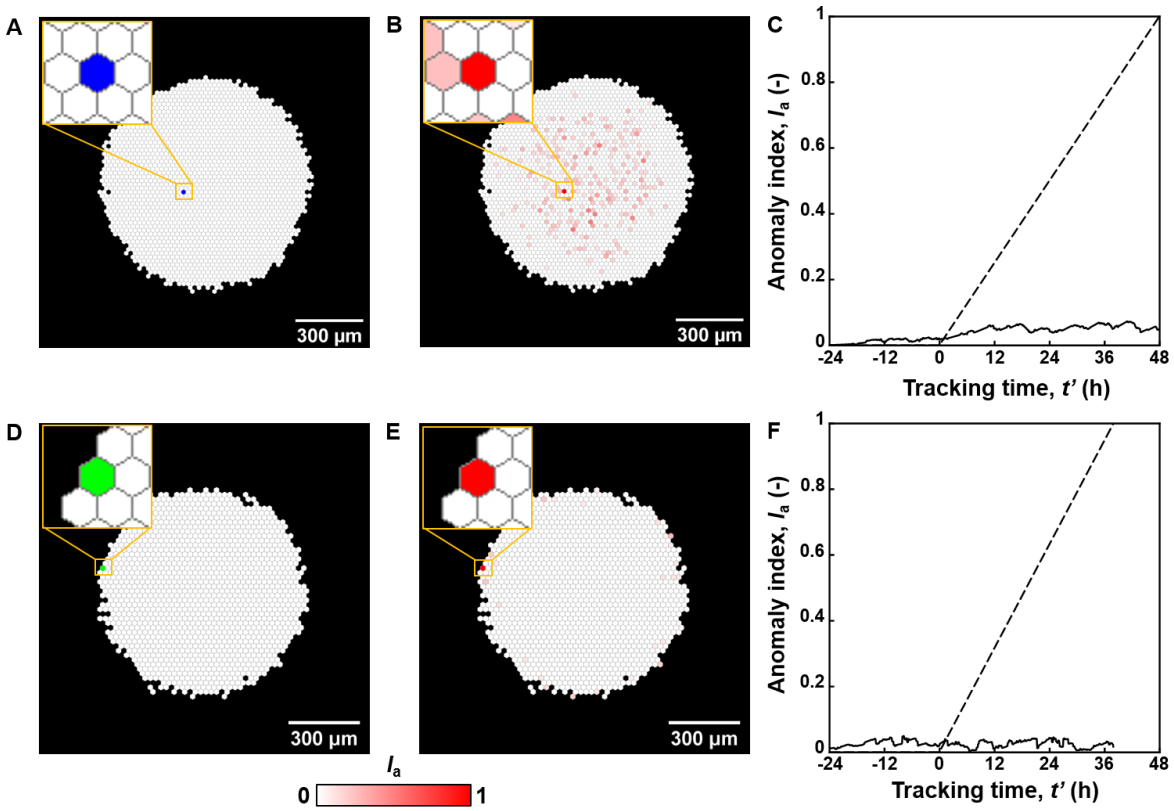

Figure 3.10 Cell type (A, D) and heat map of anomaly indices (I_a) (B, E) in culture on SNL (A, B) and MEF (D, E) feeder cells. Blue cells: cells that deviated due to low V_{app}; green cells: cells that deviated due to high V_{act}. Graphs show time profile of anomaly indices (I_a) in culture on SNL (C) and MEF (F) feeder cells. Dashed line: I_a of a deviated cell. Solid line: I_a of the deviated cell's neighbors (average from 15 colonies).

Lastly, the maximum value of I_a, $I_{a,max}$, that each cell displayed during a 96-hour culture was calculated to understand how rare the deviation trigger is. During culture, cells in vessel have different values of I_a and I_a of each cell also changes with time (**Fig. 3.11-3.12**). This parameter, $I_{a,max}$, helped to understand how close each cell had approached deviation. Histograms of $I_{a,max}$ for all cells from one representative vessel cultured on SNL and MEF feeder cells were shown in **Fig. 3.13**. The frequency decreased as $I_{a,max}$ increased in both culture conditions. Most of cells (> 96%) were found to have $I_{a,max}$ (-) values in the range of

0–0.4. An $I_{a,max}$ of 1, which indicated the appearance of deviated cell, occurred with a frequency of 3.5×10^{-5} or 2.8×10^{-5} in culture on SNL and MEF feeder cells, respectively.

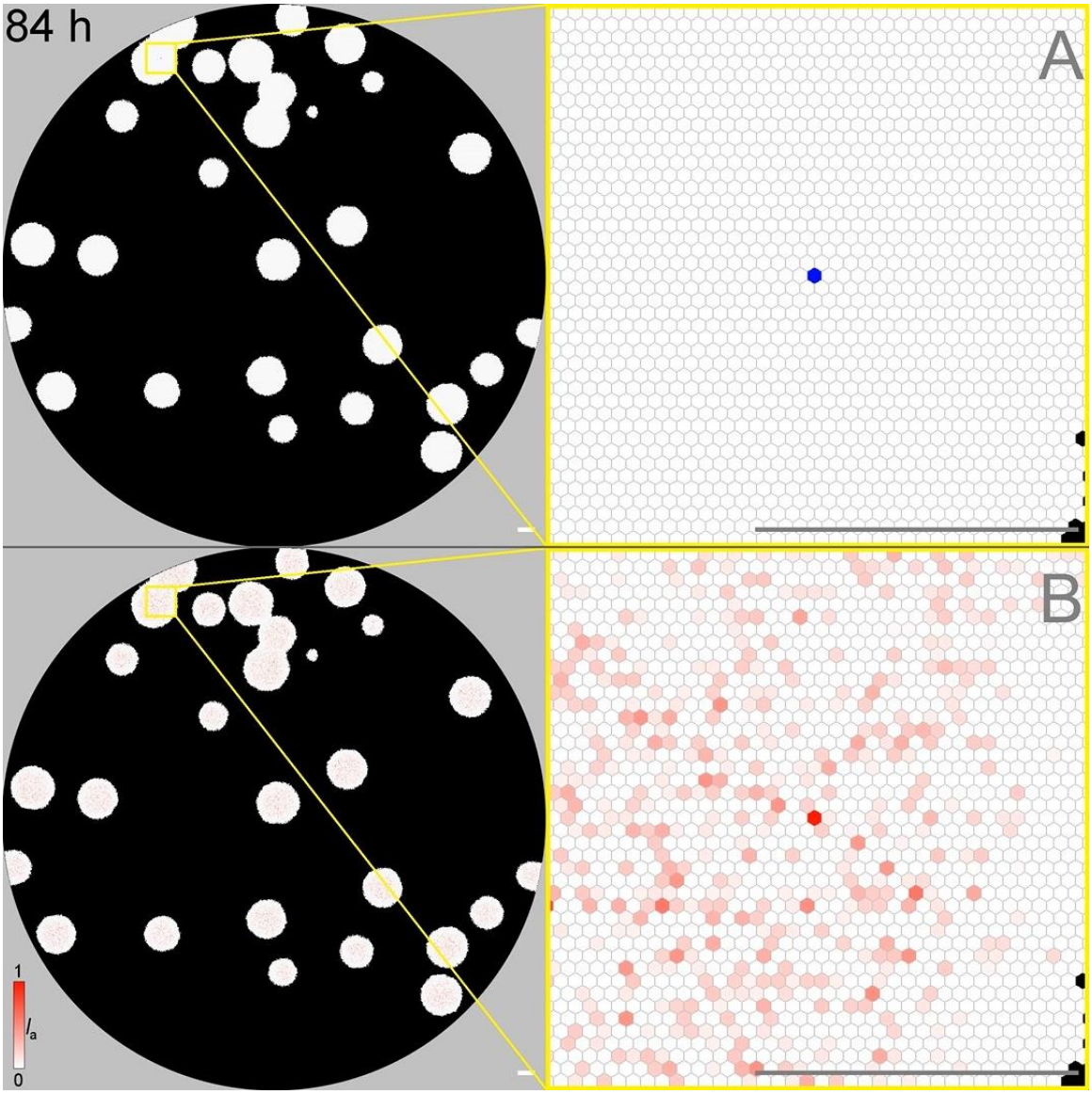

Figure 3.11 *In silico* cell type (A) and corresponding anomaly index (B) of a representative vessel with deviated cells in culture on SNL feeder cells at the time of deviation. White cells: undifferentiated cells; blue cells: deviated cells due to continuous low apparent cell movement rate; shades of red: degree of anomaly index. Scale bars: 500 µm.

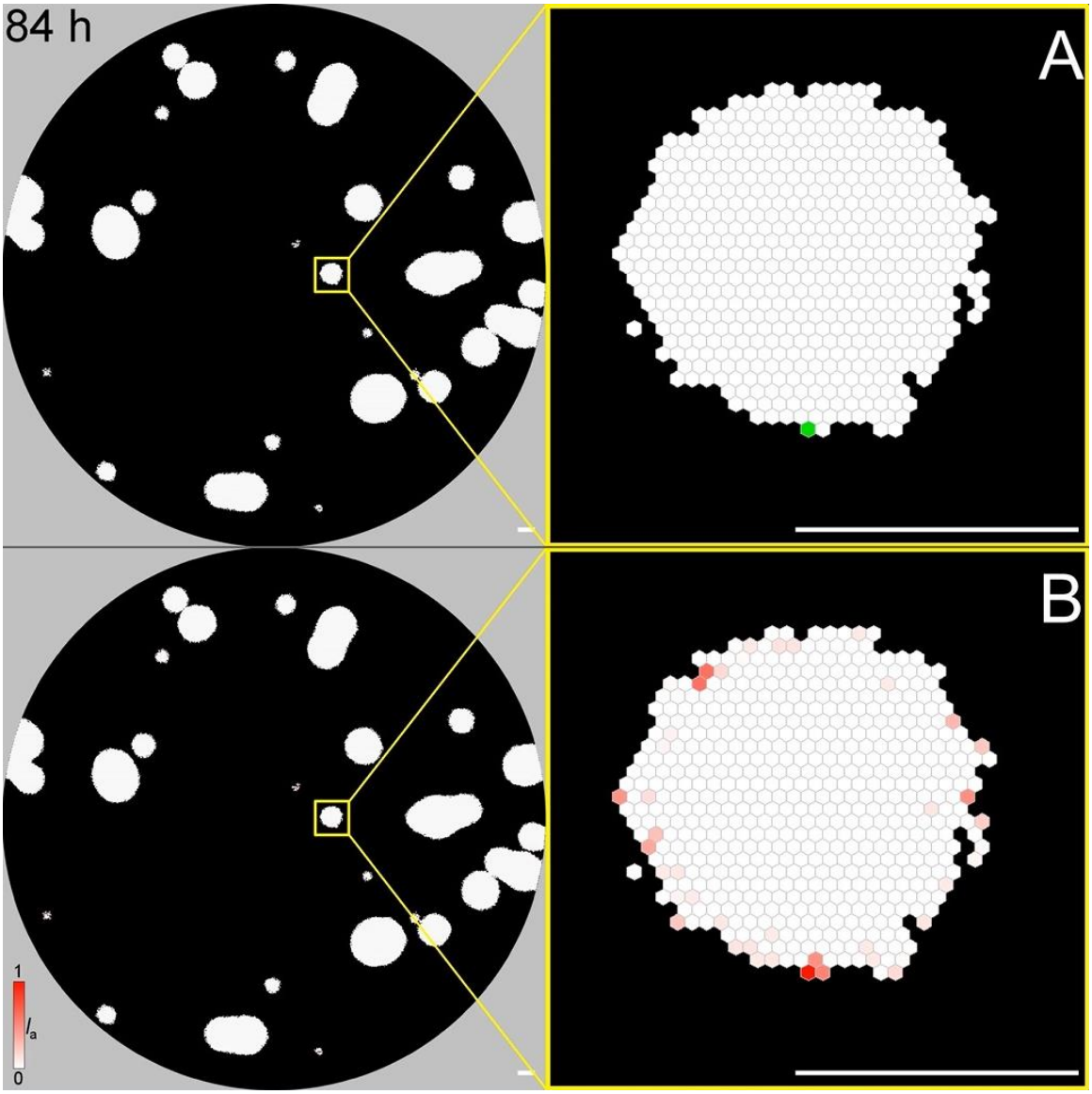

Figure 3.12 *In silico* cell type (A) and corresponding anomaly index (B) of a representative vessel producing deviated cells when cultured on MEF feeder cells at the time of deviation. White cells: undifferentiated cells; green cells: deviated cells due to continuous high movement rate caused by active migration. Shades of red: degree of anomaly index. Scale bars: 500 μm.

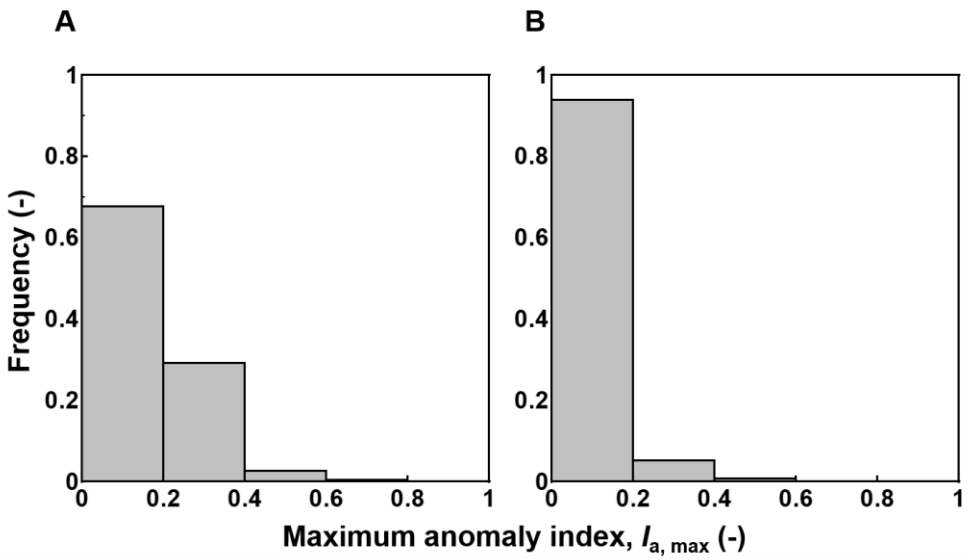

Figure 3.13 Frequency of maximum anomaly index ($I_{\mathrm{a,max}}$) of all cells from one vessel in culture on SNL (A) or MEF (B) feeder cells.

3.4 Discussion

Although anomalous *in vitro* cell migration was reported to be the trigger for deviation from the undifferentiated state of hiPSCs cultured with feeder cells (Shuzui et al. 2019a), result in chapter 2 has showed the different influences of migration and division on movement rate that raised the necessity to investigate the actual triggers. Active cell migration occurs when a cell actively changes position that relates to E-cadherin and integrin turnover and energy consumption. When a target cell actively migrates to the position of its neighboring cell, the neighboring cell undergoes passive migration at the same time. From *in vitro* observation, it is difficult to distinguish these two type of migration. In this kinetic model, I assume that passive migration requires only the disruption of cell-cell and cell-substrate connections without utilizing energy for migration. Movement caused by cell division primarily presents the breaking of cell-substrate connections, does not utilize energy, and maintains most of connections to its neighboring cells. Finally, apparent movement, the only movement type that can be estimated from *in vitro*, is similar to *in vitro* cell migration. In this chapter, apparent

movement and movement caused by active migration are suggested to trigger deviation in colony size-dependent and -independent manners, respectively. Extension of low apparent movement rates partly indicate compression in the central regions of colonies, where contact inhibition occurs with the disappearance of cell division as the colonies expand. In the peripheral region of colony, active migration is suggested to trigger deviation at the peripheral region. On the other words, high degree of cell freedom at the peripheral region of colony might result in deviation that is partly supported by the discontinued expression of E-cadherin (Kim et al. 2014).

Previously, the hypothesis that anomalous cell migration triggers hiPSC deviation has been proposed (Shuzui et al. 2019a). In that study, even though sequential cell migration could not be observed, they found the accumulation of lamin A/C at the nuclear envelope due to cytoskeletal rearrangements arising from an imbalance between cell-cell and cell-substrate adhesions. In this chapter, based on the evidence about mechano-transduction, I defined anomalous migration in terms of mechanical stimulus, presented by movement rate, and duration of the mechanical stimulus. The thresholds for mechanical stimulus were estimated from the 25th percentile value of *in vitro* cell migration, which is similar to *in silico* apparent cell movement rate, at the central region of undifferentiated colonies (Shuzui et al. 2019a), and the 75th percentile value of *in silico* movement rate caused by active migration at the peripheral region of undifferentiated colonies. The reason came from *in vitro* observation that there were significant differences ($P < 0.01$) in ratios below the 25th percentile and above the 75th percentile between undifferentiated colonies and deviated colonies (Shuzui et al. 2019a). The duration of mechanical stimulus is the original point that distinguished deviated cells from undifferentiated cells.

The colony size-dependent and colony size-independent deviation in colonies cultured on SNL and MEF feeder cells, respectively, was reported (Kim et al. 2014). This chapter partly

explained this phenomenon by the relationship between deviated cells and their microenvironment (neighboring cells) using anomaly index I_{a}. I_{a} of deviated cells at the central region increased as that of their neighbors increased with time that suggests deviated cells had been affected by their microenvironment. Thus, cells had higher probabilities of deviating as colonies became bigger. In contrast, I_{a} of deviated cells at the peripheral region had increased when their neighbors' I_{a} values fluctuated with time. Therefore I_{a} values are colony size-independent in the peripheral region of colonies.

While positive I_{a} values were distributed throughout the central and middle regions of colonies cultured on SNL feeder cells, only cells near the colony edges displayed positive I_{a} values in culture on MEF feeder cells. Therefore, the difference in frequencies of $I_{\mathrm{a,max}}$ values in the range of 0–0.2 and 0.2–0.4 in cultures on MEF feeder cells was more than that in cultures on SNL feeder cells. I considered the trigger for deviation to be ultra-rare following the definition of ultra-rare disease (i.e. a disease that affects fewer than 20 patients in a population of 1 million (2×10^{-5})) (Harari et al. 2019). Caused by ultra-rare trigger, deviation only becomes an inevitable phenomenon when the cell population is large enough. It means that the deviation is unpredictable for each colony but inevitable in a culture vessel. It is interesting that the ultra-rare trigger leads to major events in the culture of hiPSCs on feeder cells, and this major events is prohibited by altering cell-cell connection strength (Shuzui et al. 2019b). To the best of my knowledge, this is the first kinetic model expressing ultra-rare trigger in a biological system. In other studies, kinetic model has mostly been used to predict functions and the inheritability of ultra-rare genetic variants (Turkowski et al. 2017, Magri et al. 2018, Hernandez et al. 2019, Halvorsen et al. 2020).

There have been a number of models describing differentiation or loss of stem cell pluripotency considering mechano-transduction (Spector et al. 2017). Mousavi et al. (2015) proposed a model to clarify how substrate stiffness affects mesenchymal stem cells (MSCs)

differentiation during cell migration. Their models also proposed a time-dependent manner of differentiation where MSC differentiation depended on maturation time. In my model, deviation from the undifferentiated state of hiPSCs depended on the time period of slow or fast migration. While their maturation time mechanism is irreversible and makes differentiation inevitable, accumulation time of mechanical stimulus in my model is reversible that makes deviation anomalous. In 2017, a mechano-transduction model concerning how mechanical memory affected MSC differentiation was also introduced by Peng et al. In that model, they also show the importance of mechanical stimuli (substrate stiffness) and duration of mechanical stimuli (duration of the first seeding) on cell fate decisions. However, their model was not suitable for modeling our target anomalous phenomenon which required spatiotemporal analysis (Ji et al. 2017).

3.5 Summary

The apparent cell movement and cell movement caused by active migration were triggers for the deviation at the central and peripheral region of hiPSC colonies. The anomalous cell migration-driven hiPSC deviation can be explained by two factors: a mechanical stimulus, represented by cell migration, and duration of the mechanical stimulus. The factor "duration of mechanical stimulus" is the originality of this work, and helps to realize the ultra-rare trigger (approximately 10^{-5}) of deviation from the undifferentiated state in hiPSC culture.

Chapter 4 General Conclusions and Perspectives

4.1 General conclusion

Kinetic models have been used for predicting stem cell fate and providing insights into the underlying mechanism of some bioprocesses. To the best of my knowledge, the first model of stem cells described the proliferation of hematopoietic stem cells in spleen colonies (Till et al. 1963). Among models for stem cells, most of them focus on cell self-renewal, cell-fate decision, and hiPSCs derivation (Viswanathan and Zandstra 2003, MacArthur et al. 2009, Herberg and Roeder 2015).

Recently, the heterogeneity of stem cell population has received more and more attention because it directly affects the efficiency of stem cell process for application in regenerative medicine (Bratt-Leau et al. 2009, Rosowski et al. 2015). In 2019, a research by Shuzui et al. suggested that anomalous cell migration triggered the deviation from the undifferentiated state of hiPSCs in colonies cultured with feeder cells which was reported previously (Kim et al. 2014). In culture with SNL feeder cells where the deviation occurred at the central region of colony, they found more slow migrating cells at this region in deviated colonies than in undifferentiated colonies. In case of culture with MEF feeder cells where the deviation occurred at the peripheral region of colonies, they found more fast migrating cells at the peripheral region in deviated colonies than in undifferentiated colonies. However, that study could not specify the definition of anomalous cell migration due to *in vitro* technical limitations.

In this study, I used cellular automata approach to clarify the mentioned anomalous cell migration which was suggested to be the trigger for the deviation from the undifferentiated of hiPSCs. Firstly, I developed a kinetic model with fundamental behaviors of cells including cell division, cell-cell connection, cell-substrate connection, and cell migration to understand the reason for the heterogeneity of *in vitro* cell migration in colony. There is a need to distinguish

between *in vitro* cell migration and *in silico* cell migration. *In vitro* cell migration is described by the rate of cell displacement per time interval. *In silico* cell migration describes the ability of a cell to actively change its position by utilizing energy for breaking several cell-cell and cell-substrate connections and migration. From this point, *in vitro* cell migration is also affected by cell division. In chapter 2, I have found that cell division is the key factor that led to the spatial heterogeneity of *in vitro* cell migration in colony (**Fig. 4.1**).

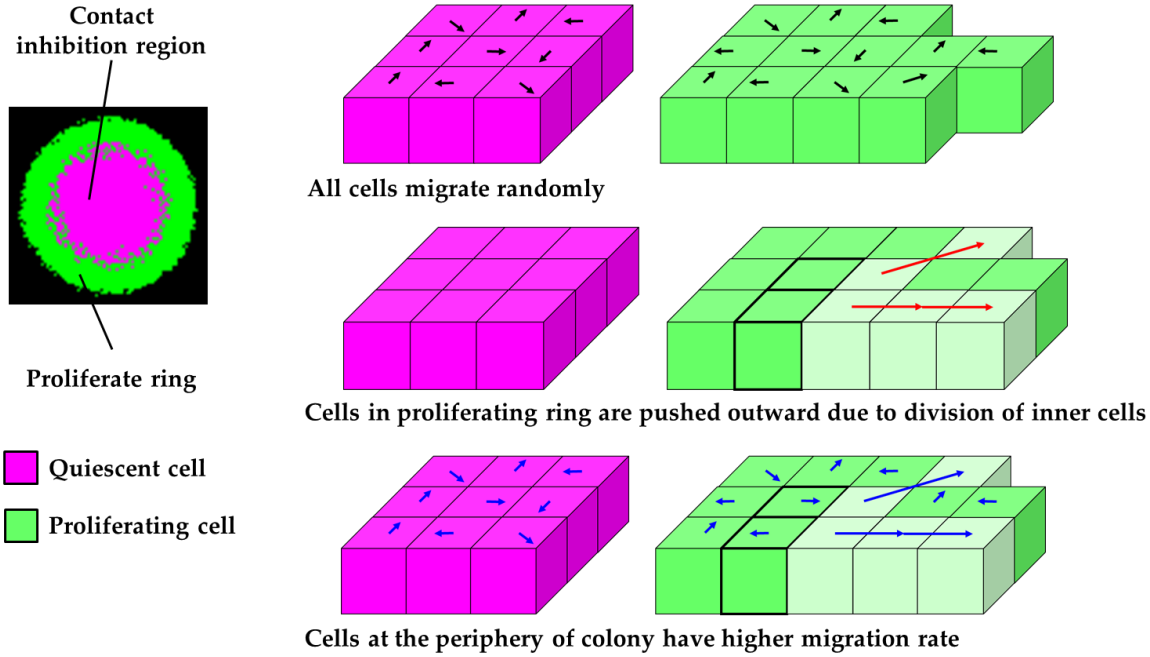

Figure 4.1 Schematic of *in silico* finding in Chapter 2 where cell division is suggested to be the key factor that leads to the spatial heterogeneity of cell migration in colonies of hiPSCs.

From result in chapter 2, I suggested the need of analyzation for the actual component of *in vitro* cell migration that could trigger deviation from the undifferentiated state. I divided into movement caused by active migration, movement caused by passive migration, movement caused by cell division, and apparent movement which has similar meaning to *in vitro* migration. From heat map of each type of movement and the colony-size independent/dependent manner of deviated colony in each culture condition with feeder cells, I suggested that apparent movement and movement caused by active migration were triggers for deviation. I hypothesized that deviation from the undifferentiated state at the central region

of colonies is triggered by the continuous low apparent movement of cells. In contrast, continuous high movement caused by active migration triggers the deviation at the peripheral region of colonies. This hypothesis was well validated by the position of deviated region in colony, profiles of deviated colonies, and the inhibition of deviation in culture on SNL feeder cells after accelerate cell migration. With the validated model, I found that deviation from the undifferentiated state was caused by the ultra-rare trigger (~10^{-5}) (**Fig. 4.2**). Until now, this is the first kinetic model that describe the ultra-rare trigger that causes anomalous phenomenon in biological field.

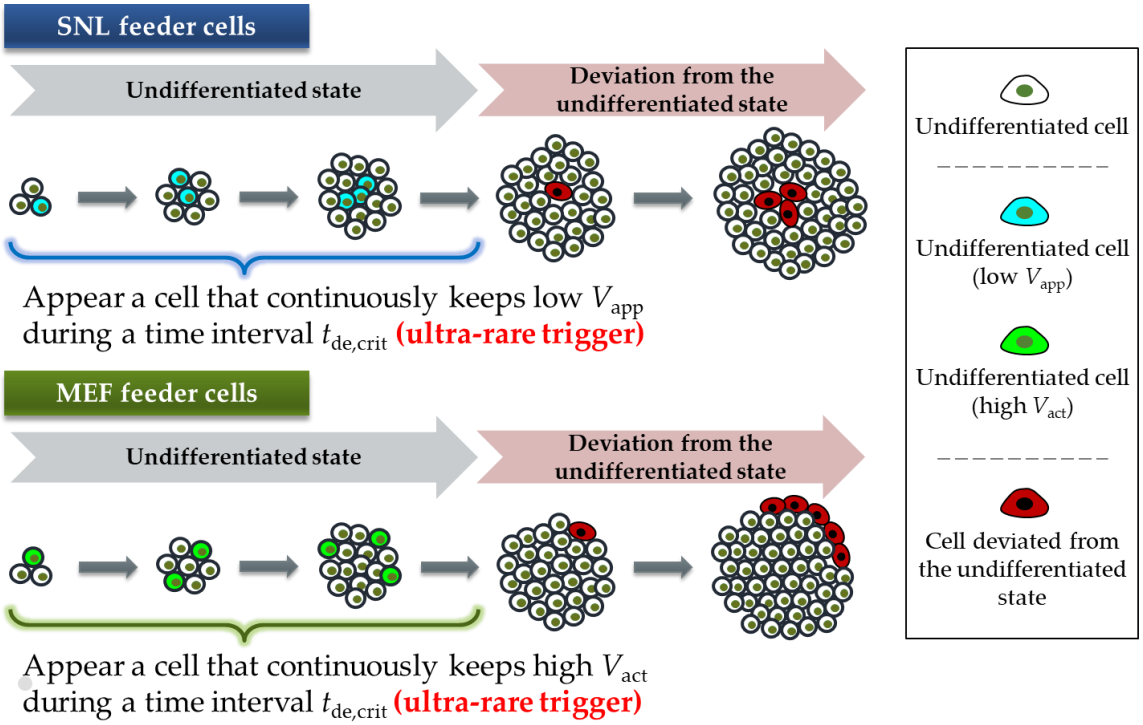

Figure 4.2 Schematic of validated *in silico* hypothesis in Chapter 3 where deviation from the undifferentiated state of hiPSCs in colonies cultured on feeder cells is explained by the continuity of low apparent movement or high movement caused by active migration which is considered as ultra-rare trigger.

4.2 Future perspectives

The developed kinetic model is suggested to be a promising tool to study different cultures of stem cells in general and hiPSCs in particular. The future perspectives are discussed as follows.

i. Optimal culture conditions for hiPSC differentiation

In previous chapters, a kinetic model was successfully developed to express the deviation from the undifferentiated state of hiPSCs in the peripheral regions of colonies cultured on MEF feeder cells. To facilitate the differentiation of hiPSCs, a culture with deviated cells as a majority of population is desired. Using the developed kinetic model, the optimized culture conditions for this goal can be found by considering effect of botulinum hemagglutinin (HA) and initial seeding size. In culture of hiPSCs on SNL feeder cells, the deviation in the central region of colony was inhibited both *in vitro* and *in silico* by addition of HA which blocks E-cadherin interactions thus loosen cell-cell connection and promote cell migration. With this effect, HA is believed to facilitate the deviation in the peripheral regions of colonies cultured on MEF feeder cells. Besides, the size of colony also affects the inward expansion of deviated region since only cells in the peripheral region of colony have possibility to deviate from the undifferentiated state. Once cells deviated from the undifferentiated state at the peripheral region of colony, they tend to detach from the colonies and thus leave more vacant space and facilitate the active migration of inner cells. Thus, the smaller colony is, the deeper deviated region can inwardly extend to the central region of colony that increases deviation frequency in the end of culture.

A preliminary experiment was performed to check the possibility of this idea. Deviation frequency and the number of doubling times, n_{d}, were used to compare the outcome of different culture conditions. The deviation frequency was calculated by the ratio between the number of deviated cells and the number of total cells in vessel at the end of culture. The number of doubling times was calculated as follows.

$$n_{\mathrm{d}} = \log_2 \frac{N_{120}}{N_{24}}$$

where N_{24} and N_{120} are the total cell number at t = 24h and t = 120h, respectively.

Firstly, keeping the initial seeding distribution as *in vitro* (μ = 133 cells/colony, σ = 126 cells/colony), cultures with and without the addition of HA were compared. The deviation frequency was 0.1% and 27%, and the n_{d} was 3.5 and 3.8 in culture without and with HA, respectively (**Fig. 4.3**). Since culture with HA gave higher deviation frequency and n_{d}, more cultures with HA were performed with different initial colony seeding size by changing the average μ and standard deviation σ of input distribution. Keeping σ at 126 cells/colony, when the average of colony size distribution μ was decreased to 66 cells/colony and 33 cells/colony, the deviation frequency were 28% and 31%, and the n_{d} were 3.8 and 3.9, respectively (**Fig. 4.4**). Therefore, μ at 33 cells/colony was chosen and σ was changed. When σ was decreased to 63 cells/colony, 32 cells/colony, and 0 cells/colony, the deviation frequency were 40%, 46%, and 73%, and the n_{d} were 3.9, 3.8, and 3.4, respectively (**Fig. 4.5**). In addition of HA, culture with the distribution of initial colony size at μ = 33 cells/colony, σ = 0 cells/colony gave the highest deviation frequency among cultures and similar n_{d} to control culture without HA (**Fig. 4.6**). This result indicated that this research direction would be promising in future.

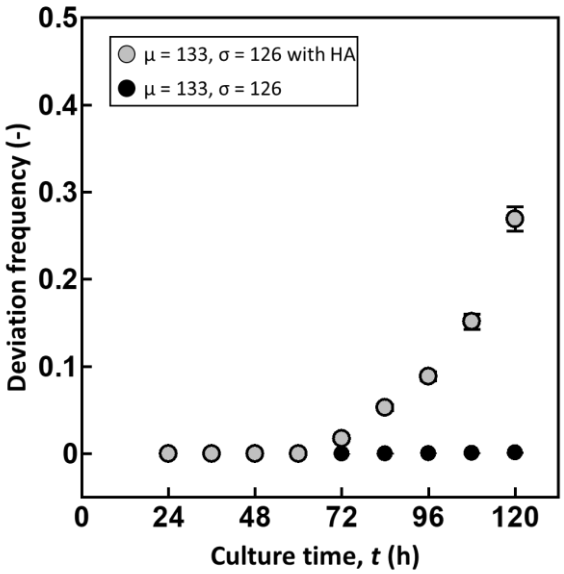

Figure 4.3 Deviation frequency in culture on MEF feeder cells under control condition (black dot) and with addition of HA (grey dot). The distribution (μ, σ) of initial colony seeding size was referred from *in vitro* data where μ = 133 cells/colony, σ = 126 cells/colony.

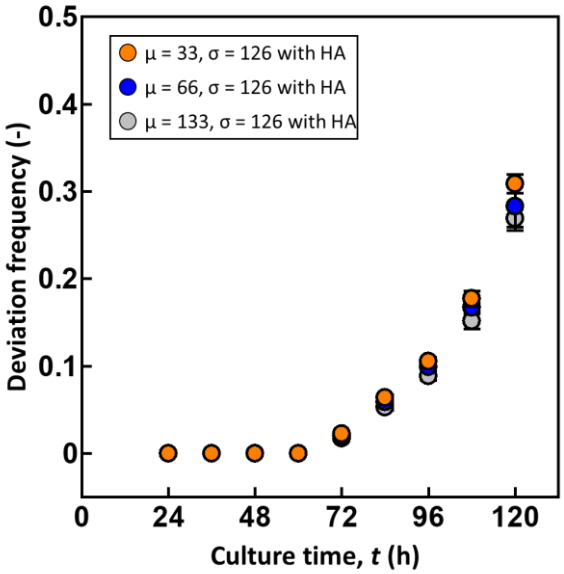

Figure 4.4 Deviation frequency in culture on MEF feeder cells with addition of HA with different distribution (μ, σ) of initial colony seeding size. Grey dot: μ = 133 cells/colony, σ = 126 cells/colony; blue dot: μ = 66 cells/colony, σ = 126 cells/colony; orange dot: μ = 33 cells/colony, σ = 126 cells/colony.

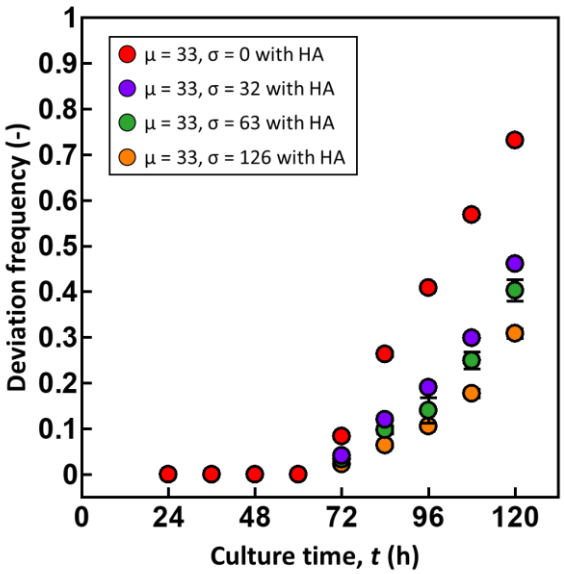

Figure 4.5 Deviation frequency in culture on MEF feeder cells with addition of HA with different distribution (μ, σ) of initial colony seeding size. Orange dot: μ = 33 cells/colony, σ = 126 cells/colony; green dot: μ = 33 cells/colony, σ = 63 cells/colony; purple dot: μ = 33 cells/colony, σ = 32 cells/colony; red dot: μ = 33 cells/colony, σ = 0 cells/colony.

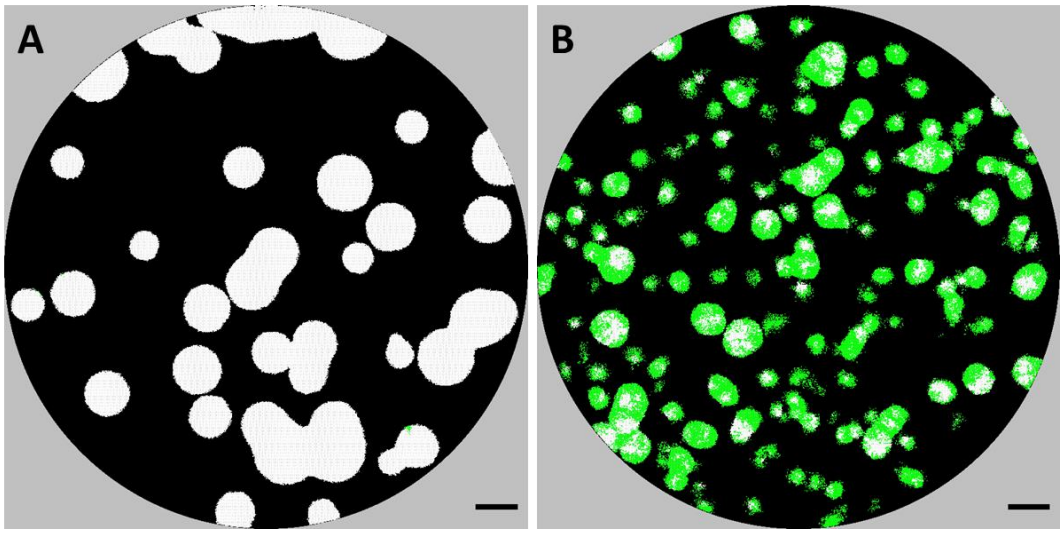

Figure 4.6 Cell type of hiPSC culture on MEF feeder cells without addition of HA (A) and with addition of HA at optimized initial colony seeding size (μ = 33 cells/colony, σ = 0 cells/colony) (B). White cells: undifferentiated cells, green cells: deviated cells due to continuous high cell movement rate caused by active migration. Scale bars show 1 mm.

ii. Understanding the mechanism of HA action

In chapter 3, the culture with addition of HA was simulated after estimation of ε_{cc}. In those experiments, we assumed that ε_{cc} of all cells is constant during culture even in culture with addition of HA. In reality, cells can recover E-cadherin after action of HA, thus strength of cell-cell connection might also change during culture. However, the lack of quantitative data of HA makes it difficult to model exact mechanism of HA action. In future, if there are more quantitative data related to HA action in hiPSC culture, it would be interesting to model the mechanism of HA action. In 2017, Kim et al. has proposed a hypothesis to explain the mechanisms underlying HA-mediated selective elimination of deviated cells cultured with SNL feeder cells. HA complexes can pass through cells (transcellular route) or between cells (paracellular route), bind to E-cadherin and disrupt E-cadherin-mediated cell-cell adhesion (Lee et al. 2014, Sugawara et al. 2014). The reason for selective removal of deviated cells is the higher ability of undifferentiated cells to recover cell-cell adhesion after HA-induced E-cadherin disruption (Kim et al. 2017).

The kinetic model might include some following parameters:

- Rate of decay of E-cadherin by HA, k_1 (cell·mol^{-1}·h^{-1}), where k_1 is positive in culture with addition of HA, but be negligible in normal culture.
- Rate of digestion of HA via endocytosis, k_2 (cell^{-1}·mol·h^{-1}).
- Rate of recover of E-cadherin of undifferentiated cells and deviated cells, k_3 (h^{-1}), where k_3 of undifferentiated cells is higher than that of deviated cells.

Then, the dynamic of ε_{cc} can be described as follows (**Fig. 4.7**).

$$\frac{d\varepsilon_{cc}}{dt} = -k_1 C_{HA}/X + k_3$$

$$\frac{dC_{HA}}{dt} = -k_2 X$$

where C_{HA} (mol/L) and X (cells/L) are concentration of HA and cell, respectively.

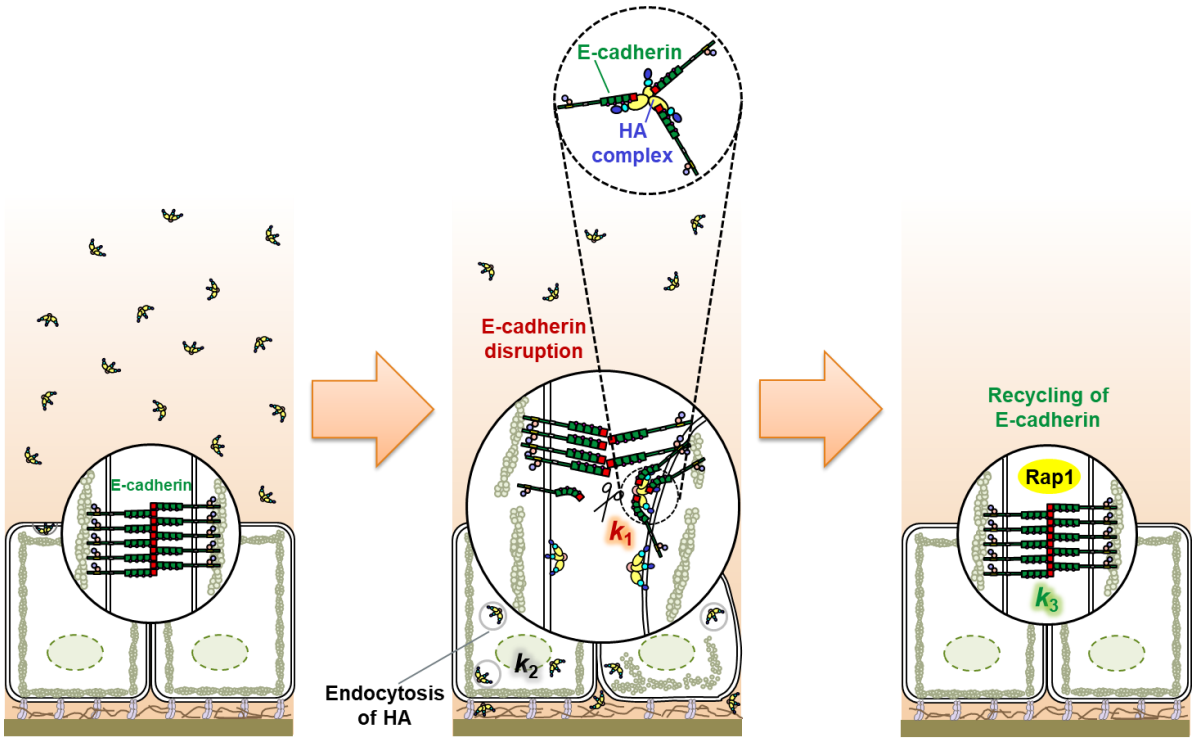

Figure 4.7 Schematic drawing describing the kinetics of cell-cell connection via action of botulinum hemagglutinin (HA) on hiPSCs.

Through two above proposals, it was expected that the developed model could be an effective tool to optimize culture conditions for maintenance of stem cell pluripotency as well as stem cell differentiation (**Fig. 4.8**). In culture with SNL feeder cells, it was suggested that HA helped to selective remove deviated cells at the central regions of colonies (Kim et al. 2017). However, over treatment with HA might induce the deviation at the peripheral regions of colonies since cell migration is accelerated. This additional occurrence of deviation at the peripheral regions of colonies cultured with SNL feeder cells was observed under exposure to Rac1 activator (HMG1) (Shuzui et al. 2019a). Therefore, there is a need to optimize the quantity of HA for each culture vessel to maintain the undifferentiated state of hiPSCs. On the other hand, deviated cells as major population could be obtained by appropriate colony size under addition of HA in order to facilitate hiPSC differentiation in culture with MEF feeder cells. With kinetic model of HA complexes, the optimized culture conditions for this purpose

can be predicted with higher accuracy. In summary, kinetic modelling of HA is necessary to optimize culture of hiPSCs in future.

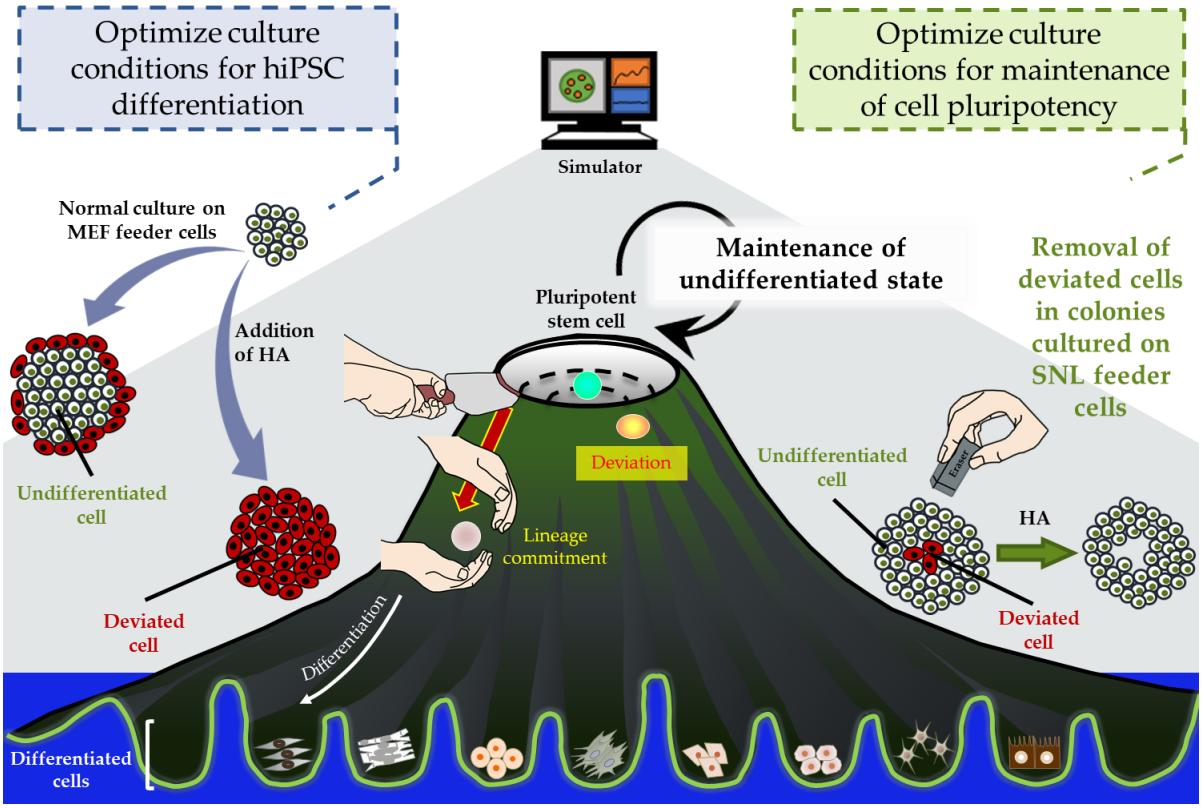

Figure 4.8 Schematic drawing describing the future perspectives of this study

Appendix

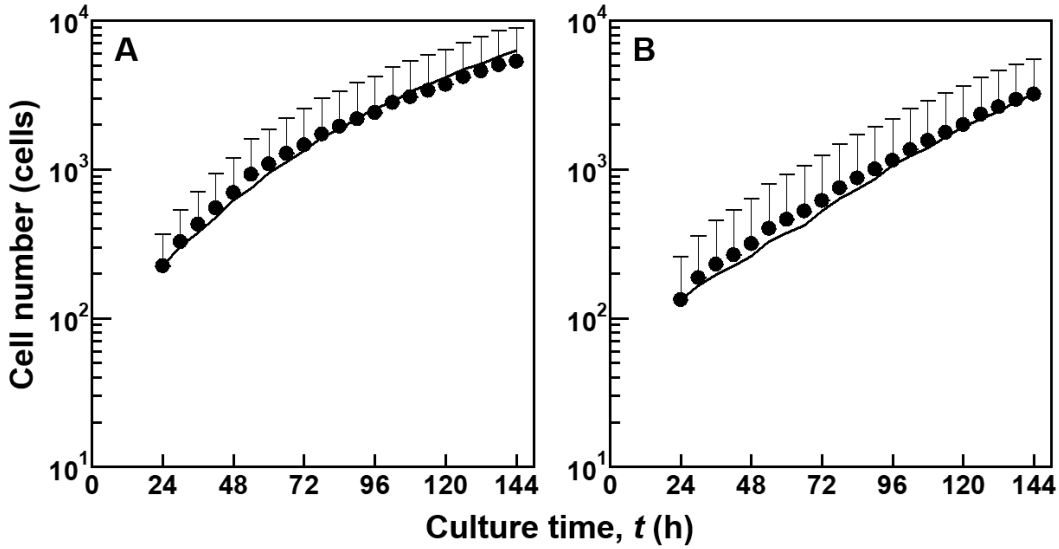

Figure S1 Estimation of N_c using curve-fitting time profiles of hiPSC colonies without deviated cells in cultures on SNL (A) and MEF (B) feeder cells. Closed circles: *in vitro* data; lines: best fit *in silico* data.

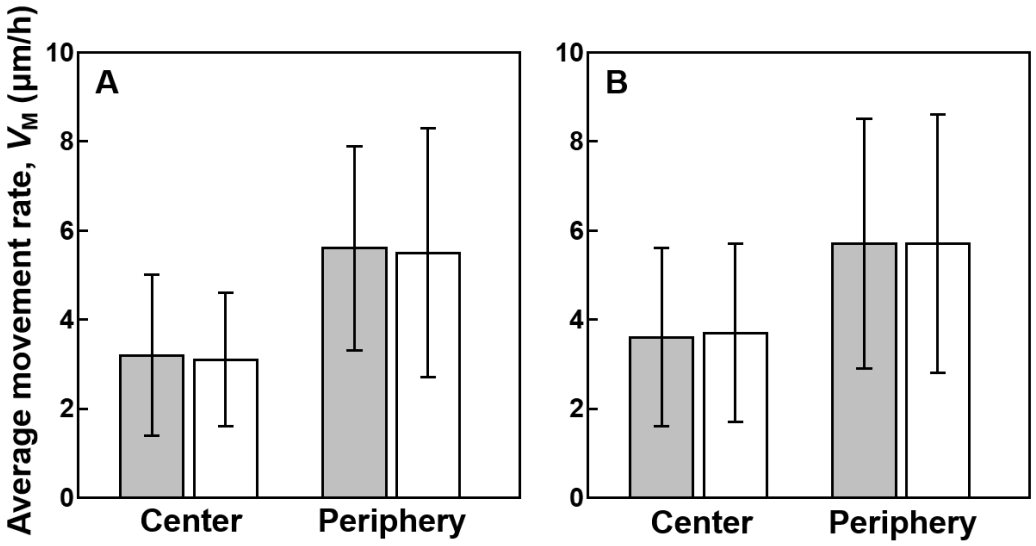

Figure S2 Estimation of $V_{m,free}$, ε_{cc}, and ε_{cs} by fitting the average cell movement rates at the central and peripheral regions of hiPSC colonies cultured on SNL (A) and MEF (B) feeder cells. Shaded bars: experimental results. Open bars: best fit simulation results obtained via least-squares fitting. Standard deviations were calculated based on all cells in a colony ($n \geq 300$)

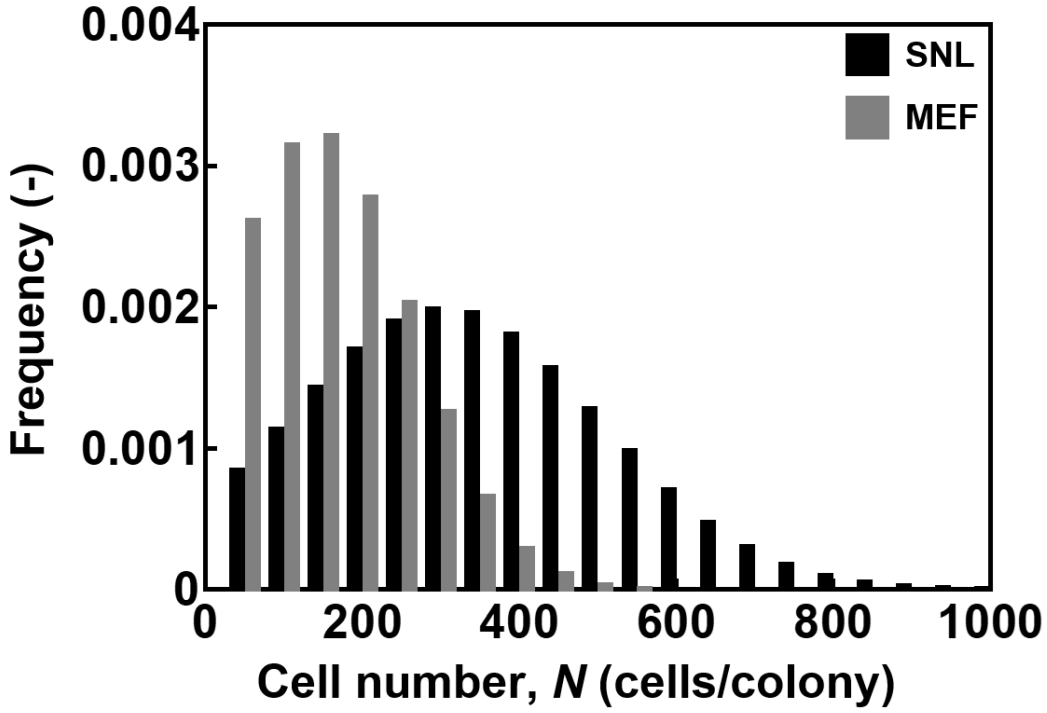

Figure S3 Distribution of *in silico* initial colony sizes. Black bar: culture on SNL feeder cells. Grey bar: culture on MEF feeder cells.

References

Aland, S., Hatzikirou, H., Lowengrub, J., and Voigt, A.: A mechanistic collective cell model for epithelial colony growth and contact inhibition, Biophys. J., 109, 1347-1357 (2015)

Arboleda-Estudillo, Y., Krieg, M., Stuhmer, J., Licata, N. A., Muller, D. J., and Heisenberg, C-P.: Movement directionality in collective migration of germ layer progenitors, Curr. Biol., 20, 161-169 (2010)

Armstrong, L., Hughes, O., Yung, S., Hyslop, L., Stewart, R., Wappler, I., Peters, H., Walter, T., Stojkovic, P., Evans, J., Stojkovic, M., and Lako, M.: The role of PI3K/AKT, MAPK/ERK and NFκβ signaling in the maintenance of human embryonic stem cell pluripotency and viability highlighted by transcriptional profiling and functional analysis, Hum. Mol. Genet., 15, 1894-1913 (2006)

Arthur, W. T., Noren, N. K., and Burridge, K.: Regulation of Rho family GTPases by cell-cell and cell-matrix adhesion, Biol. Res., 35, 239-246 (2002)

Avsec, Z., Kreuzhuber, R., Israeli, J., Xu, N., Cheng, J., Shrikumar, A., Banerjee, A., Kim, D. S., Urban, L., Kundaje, A., Stegle, O., and Gagneur, J.: Kipoi: accelerating the community exchange and reuse of predictive models for genomics, https://doi.org/10.1101/375345 (2018)

Bailey, J. E., Ollis, D. F.: Biochemical Engineering Fundamentals, McGraw-Hill, New York, 421-429 (1986)

Baldwin, C. Y., and Clark, K. B.: Design rules volume I: the power of modularity, Cambridge: the MIT Press, 471 p. (2000)

Bapat, P. M., Bhartiya, S., Venkatesh, K. V., and Wangikar, P. P.: Structured kinetic model to represent the utilization of multiple substrates in complex media during rifamycin B fermentation, Biotechnol. Bioeng., 93(4), 779-790 (2006)

Bratt-Leal, A. M., Carpenedo, R. L. and McDevitt, T. C.: Engineering the embryoid body microenvironment to direct embryonic stem cell differentiation, Biotechnol. Prog., 25, 43-51 (2009)

Byrne, H., and Drasdo, D.: Individual-based and continuum models of growing cell populations: a comparison, J. Math. Biol., 58, 657-687 (2009)

Castiglione, F., Pappalardo, F., Bianca, C., Russo, G., and Motta, S.: Modeling Biology Spanning Different Scales: An Open Challenge, Biomed Res. Int., 2014, 902545 (2014)

Checa, S., and Prendergast, P. J.: A mechanobiological model for tissue differentiation that includes angiogenesis: A lattice-based modeling approach, Ann. Biomed. Eng., 37, 129–145 (2009)

Chen, K. G., Mallon, B. S., McKay, R. D., and Robey, P. G.: Human pluripotent stem cell culture: Considerations for maintenance, expansion, and therapeutics, Cell Stem Cell., 14, 13-26 (2014)

Cheng, G. B. B., Youssef, P., Markenscoff and Zygourakis, K.: Cell population dynamics modulate the rates of tissue growth processes, Biophys. J., 90, 713–724 (2006)

Cheng, J., Nguyen, T. Y. D., Cygan, K. J., Celik, M. H., Fairbrother, W. G., Avsec, Z., and Gagneur, J.: MMSplice: modular modeling improves the predictions of genetic variant effects on splicing, Genome Biol., 20, 48 (2019)

Chowdhury, F., Li, Y., Poh, Y-C., Yokohama-Tamaki, T., Wang, N., Tanaka, T. S.: Soft substrates promote homogeneous self-renewal of embryonic stem cells via downregulating cell-matrix tractions, PLoS One, 5(12), e15655 (2010)

Chu, Y. S., Thomas, W. A., Eder, O., Pincet, F., Perez, E., Thiery, J. P., and Dufour, S.: Force measurements in E-cadherin-mediated cell doublets reveal rapid adhesion strengthened by actin cytoskeleton remodeling through Rac and Cdc42, J. Cell. Biol., 167, 1183-1194 (2004)

Cilfone, N. A., Kirschner, D. E., and Linderman, J. J.: Strategies for efficient numerical implementation of hybrid multi-scale agent-based models to describe biological systems, Cell. Mol. Bioeng., 8(1), 119-136 (2014)

Daoudi, M., Lavergne, E., Garin, A., Tarantino, N., Debre, P., Pincet, F., Combadiere, C., and Deterre, P.: Enhanced adhesive capacities of the naturally occurring Ile249-Met280 variant of the chemokine receptor CX3CR1, J. Biol. Chem., 279, 19649-19657 (2004)

Deshpande, R. S., and Spector, A. A.: Modeling stem cell myogenic differentiation, Sci. Rep., 7, 40639 (2017)

Fordyce, A. P., and Rawlings, J. B.: Segregated fermentation model for growth and differentiation of *Bacillus lichenniformis*, AlCHE. J., 42(11), 3241-3252 (1996)

Grima, R., and Schnell, S.: Modelling reaction kinetics inside cells, Essays. Biochem., 45, 41-56 (2008)

Gruebele, M., and Thirumalai, D.: Perspective: Reaches of chemical physics in biology, J. Chem. Phys., 139, 121701 (2013)

Halvorsen, M., Huh, R., Oskolkov, N., Wen, J., Netotea, S., Giusti-Rodriguez, P., Karlsson, R., Bryois, J., Nystedt, B., Ameur, A., Kähler, A. K., Ancalade, N., Farrell, M., Crowley, J. J., Li, Y., Magnusson, P. K. E., Gyllensten, U., Hultman, C. M., Sullivan, P. F., and Szatkiewicz, J. P.: Increased burden of ultra-rare structural variants localizing to boundaries of topologically associated domains in schizophrenia, Nat. Commun., 11, 1842 (2020)

Herberg, M. and Roeder, I.: Computational modelling of embryonic stem-cell fate control, Development, 142, 2250-2260 (2015)

Hernandez, R. D., Uricchio, L. H., Hartman, K., Ye, C., Dahl, A., and Zaitlen, N.: Ultra-rare variants drive substantial cis-heritability of human gene expression, Nat. Genet., 51(9), 1349-1355 (2019)

Heydari, T., Heidari, M., Mashinchian, O., Wojcik, M., Xu, K., Dalby, M. J., Mahmoudi, M., and Ejtehadi, M. R.: Development of a virtual cell model to predict cell response to substrate topography, ACS Nano, 11, 9084-9092 (2017)

Hoehme, S., Brulport, M., Bauer, A., Bedawy, E., Schormann, W., Hermes, M., Puppe, V., Gebhardt, R., Zellmer, S., Schwarz, M., Bockamp, E., Timmel, T., Hengstler, J. G., and Drasdo, D.: Prediction and validation of cell alignment along microvessels as order principle to restore tissue architecture in liver regeneration, Proc. Natl. Acad. Sci., 107(23), 10371-10376 (2010)

Huang, T-S., Li, L., Moalim-Nour, L., Jia, D., Bai, J., Yao, Z., Bennett, S. A. L., Figeys, D., and Wang, L.: A regulatory network involving β-catenin, E-cadherin, PI3k/Akt, and Slug balances self-renewal and differentiation of human pluripotent stem cells in response to Wnt signaling, Stem Cells, 33, 1419-1433 (2014)

Hwang, M., Garbey, M., Berceli, S. A., and Tran-Son-Tay, R.: Rule-based simulation of multi-cellular biological systems – A review of modelling techniques, Cell. Mol. Bioeng., 2(3), 285-294 (2009)

Jalali, A., Jones, G. F., Licht, D. J, and Nataraj, C.: Application of mathematical modeling for simulation and analysis of hypoplastic left heart syndrome (HLHS) in pre- and postsurgery conditions, Biomed Res. Int., 2015, 987293 (2015)

Jegou, A., Pincet, F., Perez, E., Wolf, J. P., Ziyyat, A., Gourier, C.: Mapping mouse gamete interaction forces reveal several oocyte membrane regions with different mechanical and adhesive properties, Langmuir, 24, 1451-1458 (2008)

Ji, Z., Yan, K., Li, W., Hu, H., and Zhu, X.: Mathematical and computational modeling in complex biological systems, Biomed Res. Int., 2017, 5958321 (2017)

Kagawa, Y. and Kino-oka, M.: An *in silico* prediction tool for the expansion culture of human skeletal muscle myoblasts. R. Soc. Open Sci., 3, 160500 (2016)

Khatau, S. B., Kusuma, S., Hanjaya-Putra, D., Mali, P., Cheng, L. Z., Lee, J. S., Gerecht, S., and Wirtz, D.: The differential formation of the LINC-mediated perinuclear actin cap in pluripotent and somatic cells, PLoS One, 7, e36689 (2012)

Kim, M. H. and Kino-oka, M.: Switching between self-renewal and lineage commitment of human induced pluripotent stem cells via cell-substrate and cell-cell interactions on a dendrimer-immobilized surface, Biomaterials, 35, 5670e5678 (2014a)

Kim, M.-H. and Kino-oka, M.: Maintenance of undifferentiated state of human induced pluripotent stem cells through cytoskeleton-driven force acting to secreted fibronectin on a dendrimer-immobilized surface, J. Biosci. Bioeng., 118, 716e722 (2014b)

Kim, M. H. and Kino-oka, M.: Maintenance of an undifferentiated state of human induced pluripotent stem cells through migration-dependent regulation of the balance between cell-cell and cell-substrate interactions, J. Biosci. Bioeng., 119, 617-622 (2015)

Kim, M. H., Masuda, E., and Kino-oka, M.: Kinetic analysis of deviation from the undifferentiated state in colonies of human induced pluripotent stem cells on feeder layers, Biotechnol. Bioeng., 111, 1128–1138 (2014)

Kim, M. H., Sugawara, Y., and Kino-oka, M.: Botulinum hemagglutinin mediated selective removal of cells deviating from the undifferentiated state in hiPSC colonies, Sci. Rep., 7, 93 (2017)

Kino-oka, M., Umegaki, R., Taya, M., Tone, S., and Prenosil, J. E.: Valuation of growth parameters in monolayer keratinocyte cultures based on a two-dimensional cell placement model, J. Biosci. Bioeng., 89, 285-287 (2000)

Koide, T., Pang, W. L., and Baliga, N. S.: The role of predictive modelling in rationally re-engineering biological systems, Nat. Rev. Microbiol., 7, 297-305 (2009)

Lee, K., Zhong, X., Gu, S., Kruel, A. M., Dorner, M. B., Perry, K., Rummel, A., Dong, M., and Jin, R.: Molecular basis for disruption of E-cadherin adhesion by botulinum neurotoxin A complex, Science, 344, 1405-1410 (2014)

Libby, A. R. G., Briers, D., Haghighi, I., Joy, D. A., Conklin, B. R., Belta, C., and McDevitt, T. C.: Automated design of pluripotent stem cell self-organization, Cell Syst., 9, 483-495 (2019)

Li, F., Redick, S. D., Erickson, H. P., and Moy, V. T.: Force measurements of the $\alpha_5\beta_1$ integrin-fibronectin interaction, Biophys. J., 84, 1252-1262 (2003)

Li, L., Wang, S., Jezierski, A., Moalim-Nour, L., Mohib, K., Parks, R. J., Retta, S. F., and Wang, L.: A unique interplay between Rap1 and E-cadherin in the endocytic pathway regulates self-renewal of human embryonic stem cells, Stem Cells, 28, 247e257 (2010)

Lutolf, M. P., Gilbert, P. M., and Blau, H. M.: Designing materials to direct stem-cell fate, Nature, 462, 433e441 (2009)

MacArthur, B. D., Ma'ayan, A., and Lemischka, I. R.: Systems biology of stem cell fate and cellular reprogramming, Nat. Rev. Mol. Cell. Biol., 10, 672-681 (2009)

Magri, C., Giacopuzzi, E., Via, L. L., Bonini, D., Ravasio, V., Elhussiny, M. E. A., Orizio, F., Gangemi, F., Valsecchi, P., Bresciani, R., Barbon, A., Vita, A., and Gennarelli, M.: A novel homozygous mutation in GAD1 gene described in a schizophrenic patient impairs activity and dimerization of GAD67 enzyme, Sci. Rep., 8, 15470 (2018)

Maherali, N., Sridharan, R., Xie, W., Utikal, J., Eminli, S., Arnold, K., Stadtfeld, M., Yachechko, R., Tchieu, J., Jaenisch, R.: Directly reprogrammed fibroblasts show global epigenetic remodeling and widespread tissue contribution, Cell stem cell, 1(1), 55–70 (2007)

Mansury, Y., and Deisboeck, T. S.: The impact of ‘‘search precision’’ in an agent-based tumor model, J. Theor. Biol., 224, 325–337 (2003)

Marchisio, M. A., Colaiacovo, M., Whitehead, E., and Stelling, J.: Modular, rule-based modeling for the design of eukaryotic synthetic gene circuits, BMC Syst. Biol., 7, 42 (2013)

Martins, M. L., Ferreira Jr., S. C., and Vilela, M. J.: Multiscale models for biological systems, Curr. Opin. Colloid Interface Sci., 15, 18-23 (2010)

McAdams, H. H., and Arkin, A.: It's a noisy business! Genetic regulation at the nanomolar scale, Trends. Genet., 15, 65-69 (1999)

McClelland, J. L., and Rumelhart, D. E.: Parallel distributed processing, Cambridge: the MIT Press, 611 p. (1995)

Meier-Schellersheim, M., Fraser, I. D. C., and Klauschen, F.: Multiscale modeling for biologists, WIREs. Syst. Biol. Med., 1, 4-14 (2009)

Metallo, C. M., Mohr, J. C., Detzel, C. J., de Pablo, J. J., Van Wie, B. J., and Palecek, S. P.: Engineering the stem cell microenvironment, Biotechnol. Prog., 23, 18e23 (2007)

Metzcar, J., Wang, Y., Heiland, R., and Macklin, P.: A review of cell-based computational modeling in cancer biology, JCO Clin. Cancer Inform., 3, 1-13 (2019)

Michaelis, L., and Menten, M. L.: Die Kinetik der invertinwirkung, Biochem. Z., 49, 333-369 (1913)

Monod, J.: The growth of bacterial cultures, Annu. Rev. Microbiol., 3, 371-394 (1949)

Moreira, J., and Deutsch, A: Cellular automaton models of tumor development: a critical review, Adv. Complex. Syst., 5, 247-267 (2002)

Moreno-Cencerrado, A., Iturri, J., Pecorari, I., Vivanco, M. D. M., Sbaizero, O., and Toca-Herrera, J. L.: Investigating cell-substrate and cell-cell interactions by means of single-cell-probe force spectroscopy, Microsc. Res. Tech, 80, 124-130 (2017)

Motta, S., and Pappalardo, F.: Mathematical modeling of biological systems, Brief. Bioinform., 14(4), 411-422 (2012)

Mousavi, S. J., and Doweidar, M, H.: Role of mechanical cues in cell differentiation and proliferation: a 3D numerical model, PloS One, 10(5), e0124529 (2015)

Nagafuchi, A., Takeichi, M.: Cell binding function of E-cadherin is refulated by the cytoplasmic domain, EMBO. J., 7, 3679-3684 (1988)

Nava-Sedeno, J. M., Vob-Bohme, A., Hatzikirou, H., Deutsch, A., and Peruani, F.: Modelling collective cell motion: are on- and off-lattice models equivalent, Phil. Trans. R. Soc., 375, 20190378 (2020)

Ohgushi, M., and Sasai, Y.: Lonely death dance of human pluripotent stem cells: ROCKing between metastable cell states, Cell, 21, 274-282 (2011)

Oliveira, L. P., Hudebine, D., Guillaume, D., and Verstraete, J. J.: A review of kinetic modeling methodologies for complex processes, Oil Gas Sci. Technol., 71, 45 (2016)

Paling, N. R., Wheadon, H., Bone, H. K., Welham, M. J.: Regulation of embryonic stem cell self-renewal by phosphoinositide 3-kinase-dependent signaling, J. Biol. Chem., 279, 48063-48070 (2004)

Peng, T., Liu, L., Maclean, A. L., Wong, C. W., Zhao, W., and Nie, Q.: A mathematical model of mechanotransduction reveals how mechanical memory regulates mesenchymal stem cell fate decisions, BMC Syst. Biol., 11, 55 (2017)

Petersen, B. K., Ropella, G. E. P., and Hunt, C. A.: Toward modular biological models: defining analog modules based on referent physiological mechanisms, BMC Syst. Biol., 8, 95 (2014)

Piotrowska, M. J., and Angus, S. D.: A quantitative cellular automaton model of *in vitro* multicellular spheroid tumour growth, J. Theor. Biol., 258, 165–178 (2009)

Qu, Z., Garfinkel, A., Weiss, J. N., and Nivala, M.: Multi-scale modeling in biology: how to bridge the gaps between scales, Prog. Biophys. Mol. Biol., 107, 21-31 (2011)

Rangamani, P., Lipshtat, A., Azeloglu, E. U., Calizo, R. C., Hu, M., Ghassemi, S., Hone, J., Scarlata, S., Neves, S. R., and Iyengar, R.: Decoding information in cell shape, Cell, 154, 1356-1369 (2013)

Resat, H., Petzold, L., and Pettigrew, M. F.: Kinetic modeling of biological systems, Methods. Mol. Biol., 541, 311-335 (2009)

Robertson, S. H., Smith, C. K., Langhans, A. L., McLinden, S. E., Oberhardt, M. A., Jakab, K. R., Dzamba, B., DeSimone, D. W., Papin, J. A., and Peirce, S. M.: Multiscale computational analysis of Xenopus laevis morphogenesis reveals key insights of systems-level behavior, BMC Syst. Biol., 1, 46 (2007)

Rosowski, K. A., Mertz, A. F., Norcross, S., Dufresne, E. R., and Horsley, V.: Edges of human embryonic stem cell colonies display distinct mechanical properties and differentiation potential, Sci. Rep., 5, 14218 (2015)

Saez-Rodriguez, J., Kremling, A., Gilles, E. D.: Dissecting the puzzle of life: modularization of signal transduction networks, Comput. Chem. Eng., 29, 619-629 (2005)

Saxena, S., Hanwate, M., Deb, K., Sharma, V., Totey, S.: FGF2 secreting human fibroblast feeder cells: A novel culture system for human embryonic stem cells, Mol Reprod Dev, 75, 1523-1532 (2008)

Serra, M., Brito, C., Correia, C., and Alves, P. M.: Process engineering of human pluripotent stem cells for clinical application, Trends Biotechnol., 30, 350-359 (2012)

Schluter, D. K., Ramis-Conde, I., and Chaplain, M. A. J.: Multi-scale modelling of the dynamics of cell colonies: insights into cell-adhesion forces and cancer invasion from *in silico* simulations, J. R. Soc. Interface, 12, 20141080 (2014)

Selekman, J. A., Das, A., Grundl, N. J., and Palecek, S. P.: Improving efficiency of human pluripotent stem cell differentiation platforms using an integrated experimental and computational approach, Biotechnol. Bioeng., 110(11), 3024-3037 (2013)

Shuzui, E., Kim, M. H., and Kino-oka, M.: Anomalous cell migration triggers a switch to deviation from the undifferentiated state in colonies of human induced pluripotent stems on feeder layers, J. Biosci. Bioeng., 127(2), 246-255 (2019a)

Shuzui, E., Kim, M-H, Azuma, K., Fujinaga, Y., and Kino-oka, M.: Maintenance of an undifferentiated state of human-induced pluripotent stem cells through botulinum hemagglutinin-mediated regulation of cell behavior, J. Biosci. Bioeng., 127(6), 744-751 (2019b)

Spector, A. A., and Grayson, W. L.: Stem cell fate decision making: Modeling approaches, ACS Biomater. Sci. Eng., 3, 2702-2711 (2017)

Steuer, R., Gross, T., Selbig, J., and Blasius, B.: Structural kinetic modeling of metabolic networks, PNAS, 103(32), 11868-11873 (2006)

Sugawara, Y., Yutani, M., Amatsu, S., Matsumura, T., and Fujinaga, Y.: Functional dissection of the *Clostridium botulinum* Type B hemagglutinin complex: identification of the carbohydrate and E-cadherin binding sites, PLoS One, 9, e111170 (2014)

Takahashi, K., Narita, M., Yokura, M., Ichisaka, T., Yamanaka, S.: Human induced pluripotent stem cells on autologous feeders, PLoS ONE, 4, e8067 (2009)

Takahashi, K., Tanabe, K., Ohnuki, M., Narita, M., Ichisaka, T., Tomoda, K., Yamanaka, S.: Induction of pluripotent stem cells from adult human fibroblasts by defined factors, Cell, 131, 861-872 (2007)

Takahashi, K., Yamanaka, S.: Induction of pluripotent stem cells from mouse embryonic and adult fibroblast cultures by defined factors, Cell, 126, 663-676 (2006)

Taya, M., Kino-oka, M., and Tone, S.: A kinetic model of branching growth of plant hairy root, J. Chem. Eng. Japan, 22(6), 698-700 (1989)

Till, J. E., McCulloch, E. A., and Siminovitch, L.: A stochastic model of stem cell proliferation, based on the growth of spleen colony-forming cells, Proc. Natl. Acad. Sci., 51, 29-36 (1963)

Torres, N. V., and Santos, G.: The (mathematical) modeling process in biosciences, Front. Genet., 6, 354 (2015)

Turkowski, K. L., Tester, D. J., Bos, J. M., Haugaa, K. H., and Ackerman, M. J.: Whole exome sequencing with genomic triangulation implicates *CDH2* -encoded N -cadherin as a novel pathogenic substrate for arrhythmogenic cardiomyopathy, CHD., 12(2), 226-235 (2017)

Villa-Diaz, L. G., Ross, A. M., Lahann, J., Krebsbach, P. H.: The Evolution of human pluripotent stem cell culture: From feeder cells to synthetic coatings, Stem Cells, 31, 1-7 (2013)

Viswanathan, S. and Zandstra, P. W.: Towards predictive models of stem cell fate, Cytotechnology, 41, 75-92 (2003)

Wang, Y., Cheng, L., Gerecht, S.: Efficient and scalable expansion of human pluripotent stem cells under clinically compliant settings: a view in 2013, Ann. Biomed. Eng., 42, 1357-1372 (2014)

Watanabe, K., Ueno, M., Kamiya, D., Nishiyama, A., Matsumura, M., Wataya, T., Takahashi, J. B., Nishikawa, S., Muguruma, K., and Sasai, Y.: A ROCK inhibitor permits survival of dissociated human embryonic stem cells, Nat. Biotechnol., 25, 681-686 (2007)

Wernig, M., Meissner, A., Foreman, R., Brambrink, T., Ku, M., Hochedlinger, K., Bernstein, B. E., Jaenisch, R.: In vitro reprogramming of fibroblasts into a pluripotent ES-cell-like state, Nature, 448, 318-324 (2007)

Wisniak, J.: Kinetic theory – From Euler to Maxwell, Indian J. Chem. Technol., 12, 730-742 (2005)

Xu, Y., Zhu, X., Hahm, H. S., Wei, W., Hao, E., Hayek, A., and Ding, S.: Revealing a core signaling regulatory mechanism for pluripotent stem cell survival and self-renewal by small molecules, Proc. Natl. Acad. Sci. USA, 107, 8129e8134 (2010)

Yachie-Kinoshita, A., Onishi, K., Ostblom, J., Langley, M. A., Posfai, E., Rossant, J., and Zandstra, P. W.: Modeling signaling-dependent pluripotency with Boolean logic to predict cell fate transitions, Mol. Syst. Biol., 14, e7952 (2018)

Yamanaka, S.: Induced pluripotent stem cells: Past, present, and future, Cell Stem Cell, 10, 678-684 (2012)

Yashiki, S., Umegaki, R., Kino-oka, M., and Taya, M.: Evaluation of attachment and growth of anchorage-dependent cells on culture surfaces with type I collagen coating, J. Biosci. Bioeng., 92, 385-388 (2001)

List of publications

Nguyen, T. N. T., Sasaki, K., and Kino-oka, M.: Elucidation of human induced pluripotent stem cell behaviors in colonies based on a kinetic model, J. Biosci. Bioeng., **127(5)**, 625-632 (2019).

Nguyen, T. N. T., Sasaki, K., and Kino-oka, M.: Development of a kinetic model expressing the anomalous phenomenon in human induced pluripotent stem cell culture, J. Biosci. Bioeng., (Available online 29 November 2020).

Acknowledgements

First of all, I would like to deeply express my gratitude to my supervisor Prof. Masahiro Kino-oka who has enlightened me to many aspects of this study with his insightfulness. With his kind guidance and encouragement, I could not only reach the targeted goal of research but also improve myself to a better person. Secondly, I would like to thank Prof. Kei Sasaki who has directed and helped me throughout my research by his interesting questions and beneficial discussions. I also would like to thank Prof. Mee-Hae Kim and Prof. Ikki Horiguchi for their valuable comments for this research.

With all of my respects, I would like to sincerely thank my sub-supervisors Prof. Omasa and Prof. Shimizu for helping me to improve my doctoral dissertation and presentation. From their kindness, careful review, and valuable comments, I would be able to see my study from other aspects and think deeper. Therefore, my doctoral dissertation is much more improved by such wonderful suggestions.

I also would like to thank for all the support, academically and mentally, from all students in my lab for the last five years. Especially, I am very thankful for my tutor Eri Shuzui who has guided me with getting familiar with hiPSCs. Without those friendship, I could not finish this research and become a stronger person as I am today. From the deepest of my heart, I appreciated that unforgettable kindness.

I would like to thank to Japanese Government for the financial support for my research and life in Japan for the last five years.

Finally, with the deepest love and appreciation, I would like to thank my family for always staying with me. Words are not enough for me to express my love for them who has been helping me to go through many hard times.